Highlights

A hybrid evolutionary algorithm for stability analysis of 2-area multi-non-conventional system with communication delay and energy storage

Aurobindo Behera,Tapas Ku Panigrahi,Subhranshu Sekhar Pati,Subhankar Ghatak,Somula Ramasubbareddy,Amir H. Gandomi

- Along with the dynamic steam turbine, in the proposed system, NCES and BSS are also considered.
- The work also considers the effect of communication delay to study the performance of the system.
- The formulated hITLBO-DE algorithm is used for tuning the designed C-PID controller.

A hybrid evolutionary algorithm for stability analysis of 2-area multi-non-conventional system with communication delay and energy storage

Aurobindo Behera[a,*], Tapas Ku Panigrahi[b], Subhranshu Sekhar Pati[a], Subhankar Ghatak[c], Somula Ramasubbareddy[d] and Amir H. Gandomi[e,*]

[a]Department of Electrical and Electronics Engineering, IIIT Bhubaneswar, Bhubaneswar, Odisha, 751003, India
[b]Department of Electrical Engineering, Parala Maharaja Engineering College, Berhampur, Odisha, 761003, India
[c]Department of Computer Science and Engineering, IIIT Bhubaneswar, Bhubaneswar, Odisha, 751003, India
[d]Department of Information Technology, VNRVJIET, Hyderabad-500090
[e]Faculty of Engineering & Information Technology, University of Technology Sydney, Ultimo, NSW 2007, Australia

ARTICLE INFO

Keywords:
Automatic Generation Control
Battery Storage System (BSS)
Cascaded Controller
hybrid Improved Teaching Learning Based Optimization and Differential Evolution (hITLBO-DE)
Non-Conventional Energy Sources (NCES).

ABSTRACT

The integration of renewable energy with the grid is essential given the environmental and economic constraints. In this work, the dynamic performance of Automatic Generation Control (AGC) was studied with a dynamic steam turbine and renewable sources. A 2-area multi-non-conventional source (Thermal-Hydro-Solar-wind-Gas-battery storage) system with communication time delay (τ) is implemented with the proposed cascaded PID (C-PID) controller scheme. The parameters of the C-PID controller were tuned by a hybrid Improved Teaching Learning Based Optimization and Differential Evolution (hITLBO-DE).

Root locus, Bode plot, and eigenvalue analysis were used to demonstrate the stability of the system. Various controllers (i.e. I, PI, PID, and C-PID) were implemented with the designed system under varying operating conditions of step (1% to 10%) and dynamic load variation (1%, $\pm$1%). The C-PID controller is able to maintain a stable system response even for τ of 4 seconds. Finally, the obtained Amelioration (%) of 55.93%, 49.03%, and 72.84% for Over Shoot emphases the efficacy of the proposed C-PID controller and hITLBO-DE algorithm.

1. Introduction

In the present day, electrical power is very essential for the day-to-day operations of every individual. An exponential increase in demand for electrical power has occured over the past decade, which has incentivized researchers to find new sources of power. Over the years fossil fuel has proven to be very efficient for production of thermal power that gets converted to electrical power in a thermal plant. However, increasing demand for power and the harmful environmental effects of excessive consumption of fossil fuel has directed researchers and innovators toward non-conventional sources. Therefore, the integration of non-conventional power sources with the existing power system has been undertaken and the effects of these integrations are being seriously studied. The existing power system is a very complex combination of various types of loads, transmission and protection equipments, and generation plants. The operation of the entire system depends mainly on the balance generation-demand. An imbalance resulting from undesirable events may lead to a system collapse/blackout. To maintain this balance, either generation or load demand can be varied forcibly. But, as the primary objective of the power system is to provide consistent and uninterrupted power with good power quality, its generation is scheduled so as to balance any change in power demand. If this balance is violated, then parameters such as frequency, voltage and current would surpass their nominal operating range [1, 2]. In this work, an Automatic Generation Control (AGC) is shown to make a significant contribution toward maintaining the generation-demand balance by conserving the frequency and tie line power at a permissible limit [3]. However, to

*Amir H. Gandomi
**Aurobindo Behera
abehera2205@gmail.com (A. Behera); tkpanigrahi.ee@pmec.ac.in (T.K. Panigrahi); sspati.4u@gmail.com (S.S. Pati); subhankar@iiit-bh.ac.in (S. Ghatak); svramasubbareddy1219@gmail.com (S. Ramasubbareddy); a.h.gandomi@gmail.com (A.H. Gandomi)
ORCID(s):

enhance the operation and maintain stability in the power system, the concept of AGC is implemented in all type of power stations.

The increased complexity of the power system requires an efficient controller in the governor system of the AGC to successfully achieve the objective. Regarding optimal control theory, numerous controllers such as the Integral (I), Proportional Integral (PI), PID, Fractional Order PID (Fo-PID), IDD, PIDD and Cascaded controllers were previously discussed by Saikia et al. [4]. Furthermore, optimizing the parameters for the controller contributes significantly to achieving effective controller operation. Many classic, heuristic and meta-heuristic techniques based on genetic evolution, and the natural behaviour of intelligent organisms have been proposed over the years for modifying essential parameters. Ali et al. [5] used the BFOA technique to address the tuning problem for the PID controller and compared it to that of the Ziegler Nichols (ZN) and GA techniques. A hybrid firefly algorithm with pattern search for tuning a PID controller in AGC was discussed by Sahu et al. [6]. Parmar et al. [7] presented a multi-source realistic model using only the output state variables for efficient output feedback control. B.K Sahu et al. [8] applied TLBO with a Fuzzy PID controller to a multi-area system. Sahu et al. [9] tuned controllers, such as IDD and PIDD, with TLBO to stabilize a simple 2-area thermal system and also discussed a diverse source system. Dash et al. [10, 11] proposed a cascaded PD-PID controller [10] that is tuned by the BAT algorithm and the PI-PD controller [11] tuned by flower pollination algorithm that enhanced the response of the multi-area system. Elsis et al. [12] implemented the BAT algorithm for tuning the model predictive control of the referred system including an energy storage unit. Simhadri et al. [13] implemented a whale algorithm to achieve optimal control of a 2DOF controller with a system state feedback. Arya et al. [14] discussed a hydrothermal multi-source restructured system connected through alternating/direct current parallel links and analysed the effect of various system parameters. Arya et al. [15] proposed an improved optimal control strategy for regulating an AGC system. Shankar et al. [16] integrated a UPFC in each area along with alternating/direct current parallel links and optimized the parameters of the proposed controller with the fruit fly algorithm and compared it to particle swarm optimization. Wang et al. [17] proposed a Hybrid Energy Storage System (HESS) through application of a adaptive sliding mode control. Wang et al. [18] discussed the future possiblity of increasing the fuel efficiency of unmanned aerial vehicles (UAVs) and the challenges. Panigrahi et al. [19] proposed the use of Kalman filter for developing a self-tuning optimizer for voltage flicker and harmonic estimation. Xiang et al. [20] proposed a economic dispatch in hybrid power system by imposing switching constraints for minimizing frequent switching. Barisal et al. [21] demonstrated a hybrid DEO-LEVY flight algorithm tuned fuzzy-PID controller for a multi-area system with automatic generation control. Based on this survey of recent works, it is apparent that the design of a controller along with the tuning technique that are preferred for generating an array of optimal controller constraint affect the operation of the system.

1.1. Motivation and contribution

Based on the survey of recent works presented above, it is apparent that few researchers have studied the simultaneous integration of multiple non-conventional sources with the existing power system and the transmission delay caused by the process. For a thermal power plant, Pathak et al. [22] proposed a dynamic turbine model through the analysis of the heat balance data. This led to an accurate and realistic estimation of the thermal power plant. Pathak et. al. [23] redefined discrete AGC modelling and discussed the effect of transmission delay on a multi-source system comprised of steam, hydel and gas plants. The motivations for the work are as follows:

1. Design and analysis of a multi-area renewable source system with various real time nonlinearities, zero order hold and transportation delay is essential to understand the stability of the system.
2. A controller and optimization algorithm must be formulated so as to improve the stability and economics of the designed multi-area renewable source system.
3. The effects of time delay on a zero order hold (ZOH) circuit along with the dynamic steam turbine model regulated by the formulated C-PID controller must be studied.

The objectives of the work presented in this paper can be briefly summarized by the following points.

1. Formulation of a 2-area multi-non-conventional source system with BSS, communication delay and implementation of a modified C-PID controller with appropriate positioning of a ZOH circuit.
2. Testing the proposed hITLBO-DE techniques by applying them to various unconstrained and constrained benchmark functions.
3. Optimization of the gains for the suggested controller using hITLBO-DE techniques and comparing it to various controllers such I, PI, PID, PIDD, IDD.

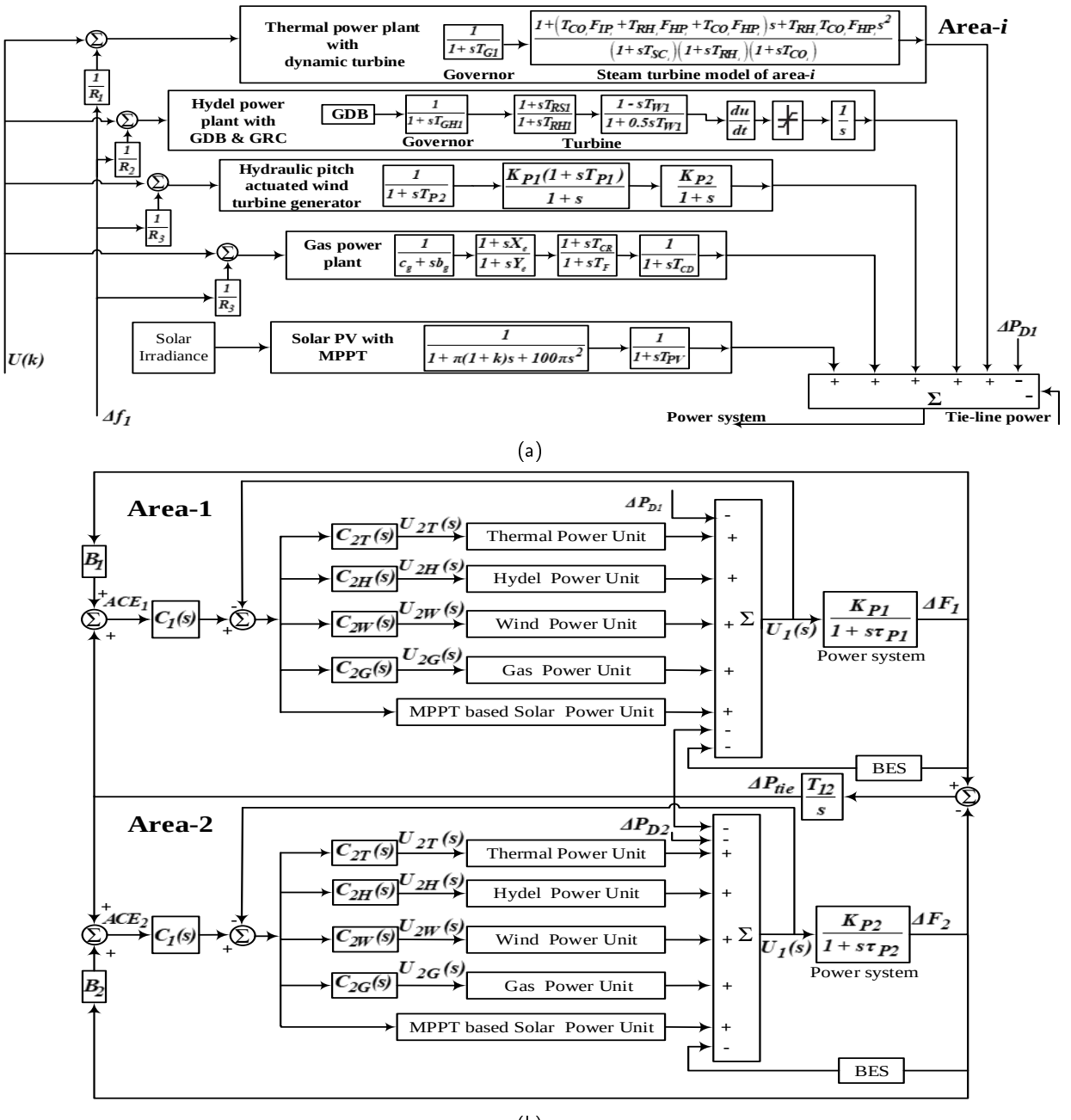

Figure 1: Transfer function and block diagram model for 2-area multi-non-conventional source system (a) internal configuration for area-i (b) system diagram with proposed scheme of controller and battery energy storage.

4. To study the system stability by Root Locus, Bode Plot and Eigen value analysis with step load (Case-I, II, III, and IV), time varying load (Case-V, VI, and VIII) perturbation, and the effect of transport delay and BSS on the system response against step load condition.

1.2. Approach for validating the proposed scheme

The hITLBO-DE technique used for tuning the controller was initially subjected to unconstrained and constrained benchmark functions. The suitability of the technique was proven and therefore was applied to the traditional cascaded

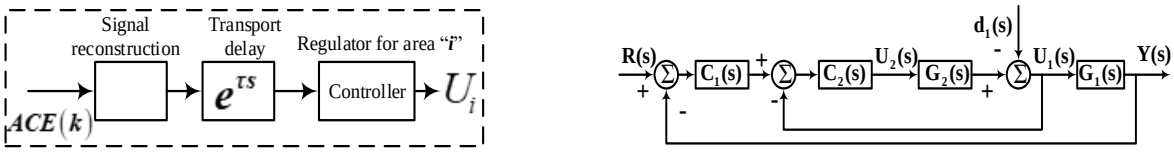

Figure 2: (a) Regulator with Zero Order Hold (ZOH) circuit. (b) Block diagram representation of the traditional cascaded controller.

controller for a dynamic turbine system. A stability analysis was conducted for the dynamic turbine thermal system using methods such as Eigenvalue, Root Locus, and Bode Plot analysis. Four different cases of step load variation and three cases of dynamic load variation were applied to the studied system in order to prove the ability of the suggested organization of controller and optimization module. Comparison of the obtained results to the results generated by system models discussed in [22], [23] suggests excellent system operation.

In Section-2 modelling of the dynamic turbine parameters and renewable sources is discussed along with appropriate transfer function and block diagrams, as shown in Fig. 1. In Section-3 the formulation and implementation of a traditional cascaded controller (Fig. 2b), and proposed controller design (Fig. 1b), and their mathematical formulation are discussed. The efficacy of ISTSE as compared to various error functions is elaborated upon in Section-4. The hybrid ITLBO-DE algorithm is discussed in Section-5. In Section-5, benchmark testing of the optimization technique and convergence graph is presented in order to display the efficacy of the proposal. The performance and stability analysis of the 2-area system are elaborated upon in Section-6 with the help of tables and figures. In Section-6, results of various stability analyses such as root locus, bode plot, and eigen value analysis are presented and a comparative analysis of the system response is conducted. Conclusions of this work are briefly discussed in Section-7. The values of the parameters discussed in Section-2 are presented in the Appendix in Section-8.

2. Model for the considered power sources

In this paper, a 500MW capacity dynamic thermal power plant is considered in each area of the proposed model, and is depicted in Fig. 1a.

2.1. Modelling of a dynamic turbine

All the required parameters of the thermal unit were computed based on actual running plant [22]. B_1 and B_2 represent the frequency bias parameter. The governor equivalent speed regulation parameter is denoted as R_{eqv}. The governor time constant is represented as T_g. Similarly T_{SC}, T_{RH} and T_{CO} denote the time constant delay because of steam chest, re-heater, and cross over inlet piping respectively. The fraction of power F_{HP}, F_{IP}, and F_{LP} refer to a high, intermediate and low pressure turbine, respectively, which combines to generate the total power. α_{ij} represents the areas capacity ratio. K_{pi} and T_{pi} correspond to power system rotating mass gain and time constant, respectively. ΔP_{di} represents the step load perturbation of i^{th} area. T_{12} is the synchronizing coefficient, ΔP_{Tie} represents the incremental change in tie line power, and ΔF_1 and ΔF_2 are the frequency deviation in area-1 and 2, respectively. All estimated data are shown in Appendix A.

Most researchers have predominantly focused on primary and the secondary control, based on previous publications. Researchers have not considered changes in system dynamics when subjected to a different generation schedule. The first step toward this concept was taken by Pathak et al. with limited analysis. There are no reports on system stability in terms of root locus, bode plot, and Eigen vector analysis for the developed dynamic thermal system.

The equivalent transfer function of reheat tandem compound steam turbine [22], [23] is given by Equation (1).

$$G_{Reheat} = \frac{(F_{HP} + F_{IP} + F_{LP}) + (T_{CO}F_{IP} + T_{RH}F_{HP} + T_{CO}F_{HP})s + T_{RH}T_{CO}F_{HP}s^2}{(1 + sT_{sc})(1 + sT_{RH})(1 + sT_{CO})} \tag{1}$$

The sum of F_{HP}, F_{IP} and F_{LP} is one; thus, Equation (1) can be re-written as:

$$G_{Reheat} = \frac{1 + (T_{CO}F_{IP} + T_{RH}F_{HP} + T_{CO}F_{HP})s + T_{RH}T_{CO}F_{HP}s^2}{(1 + sT_{sc})(1 + sT_{RH})(1 + sT_{CO})} \tag{2}$$

For finding the time constant of steam chest, re-heater and cross over, the mass continuity equation is used, as shown below.

$$T_V = \frac{P_0}{Q_0} V_{vessel} \times K_{vessel} \; ; \;\; where \; K_{vessel} = \frac{\delta \rho}{\delta P_0} \mid_{T^o c} \tag{3}$$

Here, T_V and Q_0 represent the vessel steam flow time constant and the flow rate in *Kg/sec*, respectively. The volume of the vessel is V_{vessel}. K_{vessel} is the alteration in steam density with respect to P_0 at a fixed temperature. P_0 is the pressure of the steam in the vessel.

The power fraction F_{HP}, F_{IP}, and F_{LP} with respect to total power can be written as shown in Equation (4).

$$\frac{F_{LP}}{F_{HP}} = \frac{P_{LP}}{P_{HP}} = a_1 \; ; \;\; \frac{F_{IP}}{F_{HP}} = \frac{P_{IP}}{P_{HP}} = a_2 \tag{4}$$

P_{LP}, P_{IP}, and P_{HP} is the power developed by the low, intermediate, and high pressure turbine, and can be computed by using the heat balance diagram. The power developed is generally represented by Equation (5).

$$P_X = \sum_{K=1}^{n} Q_K (h_{in,K} - h_{out,K}) \tag{5}$$

P_X is the output power. X represents LP, IP, and HP turbines. Q_K is the flow rate. $P_{in,K}$ and $h_{out,K}$ are the inlet and outlet enthalpy at K^{th}, stage respectively. Using (4) and (5), the power fraction can be calculated using (6).

$$F_{HP} = \frac{1}{1 + a_1 + a_2} \; ; \;\; F_{IP} = \frac{a_2}{1 + a_1 + a_2} \; ; \;\; F_{LP} = \frac{a_1}{1 + a_1 + a_2} \tag{6}$$

In addition to the dynamic steam turbine, this paper also incorporated a ZOH circuit, as shown in Fig.2b, at the appropriate location as described in [23].

2.2. Modelling of multi-non-conventional sources

Sisodia et al. [24] elaborated upon the development of renewable energy in India. Sisodia et al. conclude that the energy market has not sufficiently been explored, and a higher growth in demand is observed since 2008. Lolla et al. [25] assessed the potential of solar-wind and possible grid integration in India. Lolla et al. suggested that the southern, western, and eastern region are most potent in terms of availability of renewable sources. Sopian et al. [26] described a hybrid wind-solar model and studied its design and possible use for household application. Kadri et al. [27] discussed the possibilities and methodologies for integrating solar power into the grid with maximum power point tracking. Rezkallah et al. [28] described an approach that implements Lyapunov function with a sliding mode control for the same scenario. The complexity of the power system cannot be handled manually; thus, a controller is required for completing the control action. An optimization technique has to be applied in order to obtain an optimum controller setting for the efficient operation of the AGC.

The work was composed of a dynamic steam turbine along with a hydro plant, a wind turbine generator with pitch controller, a solar photovoltaic plant considering the maximum power point tracking, and a gas power plant that are elaborated upon in Fig. 1. Fig. 1(a) shows the internal transfer function model of the individual sources. Fig.1(b) shows the configuration of the 2-area system that was integrated with a dynamic steam turbine and various non-conventional sources. Redox flow battery (RFB) was also integrated into the model for nullifying the power mismatch of generation and demand, which improved the efficiency of the integrated non-conventional power sources. Natural resources such as solar radiation and wind speed are beyond the control of system regulators. The distinctive gain and time constant of the different functionalities are presented in this section and the values are listed in the appendix.

Deriving power from the flow of water is a primitive and mature technology. A hydro power plant serves as a peak load plant by supplying power during peak hours. This plant is included in the model, as shown in Fig. 1. However, appropriate nonlinearity (i.e. Governor Dead Band (GDB)) of 0.02% is taken in hydro unit. Generally, GDB is defined as the time period for which there is no control mechanism for the valve position in the governor due to the presence of a mechanical support arrangement. Power generation from a hydro unit can be increased or lowed at a specified rate called the generation rate constant (GRC). A GRC of 360% per minute is considered for increasing the generation and 270% for lowering the generation.

Due to its many advantages, the use of WTG continues to increase day-by-day. It has been also reported that the technology involved in generation is mature and its presence has been multiplied by 21% annually in recent years. The dynamic interaction of pitch control of WTG is complex in nature due to the presence of a supplementary control loop; it is comprised of a transducer, set point control governed through manual operation, controller feedback operation, and a hydraulic pitch actuator that regulate the pitch angle of WTG. The transfer function of the Hydraulic Pitch Actuator (HPA) is given by

$$G_{HPA} = \left[\frac{1}{1+s\tau_{P_2}}\right] \left[\frac{k_{P1}(1+s\tau_{P_1})}{1+s}\right] \tag{7}$$

$$G_{DPR} = \left[\frac{k_{P2}}{1+s}\right] \tag{8}$$

Where K_{Pi} and T_{Pi} represent the gain and time constant of the actuator [29]. Similarly, the transfer function of Data Pitch Response (DPR) is given by Equation (8).

Energy derived from a solar PV plant also supports the growth of clean energy that will reduce the harmful impact on the environment caused by fossil fuel burning power generation units and will boost the energy sufficiency. The deduced transfer function of a solar PV plant was derived using Blacks formula with tachometric reaction [28] is represented in Equation (9).

$$TF_{Solar} = \frac{1}{[100\pi\tau_{PV}s^3 + [100\pi + \pi\tau_{PV}(1+k)]s^2 + [\pi(1+k) + \tau_{PV}]s + 1]} \tag{9}$$

In fossil fuel rich countries, natural gas is easily available and is used to generate electricity. The detailed transfer function of a gas operated generator was well addressed by Dahiya et al. [30] and Hota et al. [31] The parameter range is given in the appendix.

To maintain stability of the frequency, it is necessary to include energy storage system in AGC. Especially, in the present power system, that is integrated with multiple non-conventional sources. Dhundhara et al. [32] evaluated the effects of doubly fed induction generators (DFIGs) and capacitive energy storage (CES) on a 2-area system with thermal-hydro-gas units. They concluded that energy storage units provide a faster response as compared to a renewable source when subjected to a load perturbation. Thus, RFB is included in this model, as it operates more efficiently than other storage such as super magnetic energy storage (SMES) and ultra-capacitor (UC). During low leading, battery storage swiftly delivers power so that the frequency is maintained at a permissible limit. The dual converter placed in the RFB modelling serve as both inverter and rectifier action. During operation, the change of power output is given as:

$$\Delta P_{RFB} = \frac{K_{RFB}}{1+sT_{RFB}} \tag{10}$$

where, K_{RFB} and T_{RFB} are the gain and time constant of redox flow battery, respectively.

3. Controller design formulation

This section discusses the structure of the traditional cascaded controller. As the system configuration becomes more complex, the selection of a robust controller becomes vital to the system because it maintains system stability. The PID controller is a simple and effective controller that is mainly used in the process and automation industry. In the current environment, it faces enhanced challenges caused by the innovative source integration and complex non-linearities of the system.

3.1. Traditional cascade controller

Dash et.al [10, 11] presented a scheme in which a PI-PD and PD-PID cascaded controller was subjected to multi-source system. In this work, the traditional cascaded controller was demonstrated to be able to sustain system stability. The major advantage of the controller is its design, which divides the entire system into two separate loops (inner and outer loops) and assigns two individual controllers to it. Thus, the entire process of system regulation is effective and

faster as compared to the traditional PID controller. The primary loop is the master controller and the secondary loop is the slave controller that are highly dependent on the output of the governing system and the control signal from the master controller.

A generalised cascade PID controller is shown in Fig. 2b, which was found to be a consistent and potent controller when subjected to disturbances. The cascade controller has two closed control loops, $C_2(s)$ as an internal loop and $C_1(s)$ as an external loop. The primary objective of $C_1(s)$ is to regulate the final response ($Y(s)$). $C_2(s)$ governs the operation of the prime mover. Based on Equations (11), (12), and (13), the mathematical modelling presented in Fig. 2(b) can be appropriately depicted. $R(s)$ and $d(s)$ are the reference signal and disturbance signal, respectively. As the inner and outer loop are proposed to be a PID controller $C_1(s) = C_2(s)$ as shown in Equation (14). Substituting $R(s)$ with the Area Control Error for i^{th}-area (ACE_i), $d_i(s)$ by the load demand perturbation for i^{th}-area (ΔP_{di}) and considering that $C_1(s) = C_2(s)$, Equation (13) can be re-written as Equation (15).

$$Y(s) = G_1(s)U_1(s) + d_1(s) \tag{11}$$

$$Y_2(s) = G_2(s)U_2(s) \tag{12}$$

$$Y(s) = \left[\frac{G_1(s)G_2(s)C_1(s)C_2(s)}{1 + G_2(s)C_2(s) + G_1(s)G_2(s)C_1(s)C_2(s)}\right] R(s) - \left[\frac{G_1(s)}{1 + G_2(s)C_2(s) + G_1(s)G_2(s)C_1(s)C_2(s)}\right] d_i(s) \tag{13}$$

$$C_1(s) = \ C_2(s) = K_p + \frac{K_i}{s} + K_d \ s \tag{14}$$

$$Y(s) = (ACE_i.e^{\tau s}) \left[\frac{G_1(s)G_2(s)C_1^2(s)}{1 + G_2(s)C_2(s) + G_1(s)G_2(s)C_1^2(s)}\right] - \Delta P_{di} \left[\frac{G_1(s)}{1 + G_2(s)C_2(s) + G_1(s)G_2(s)C_1^2(s)}\right] \tag{15}$$

Here, $G_1(s)$ is system inertia and $G_2(s)$ is a combination of governor and dynamic steam turbine, as given by Equation (16).

$$G_1(s) = \frac{K_{pi}}{1 + T_{pi}}; \quad G_2(s) = \frac{1}{1 + sT_{gi}} G_{Reheat} \tag{16}$$

3.2. Proposed modified C-PID controller design

Fig. 1b shows the proposed controller structure that is used in the system for precisely curbing system instability within the restricted range while not violating the system economy. Equation (14) is used in the proposed PID-PID cascade controller.

The inner process $Y_2(s)$ in Equation (12) was modified to produce Equation (17), according to the proposed design. Here, ΔP_{Di} is the disturbance signal for which the stability of the system was analyzed.

$$U_1(s) = \ Y_2(s) = C_{2Th}(s)G_{2Th}(s) + \ C_{2Hy}(s)G_{2Hy}(s) + C_{2W}(s)G_{2W}(s) + \ \Delta P_{Di} \tag{17}$$

$$Y(s) = \left[\frac{C_1(s)G_1(s)G_{In}}{1 + G_{In} + C_1(s)G_1(s)G_{In}}\right] R(s) - \left[\frac{G_1(s)}{1 + G_{In} + C_1(s)G_1(s)G_{In}}\right] d_i(s) \tag{18}$$

$$G_{In} = C_{2T}(s)G_{2T}(s) + C_{2H}(s)G_{2H}(s) + C_{2W}(s)G_{2W}(s) + C_{2G}(s)G_{2G}(s) \tag{19}$$

Equation (18) characterizes the final control action of the multi-non-conventional source system with reference signal ($R(s)$) and disturbance signal (ΔP_{Di}). The exploration of the controller operation is performed as per the block diagram shown in Fig.1b. The overall transfer function given by Equation (13) and 15 were modified to form Equation (18),

considering the proposed scheme. The parameter G_{In} in Equation (18) is given by Equation (19). Furthermore, by considering Equation (14), the error input (ACE_i) and load variation (ΔP_{Di}), Equation (18) and (19) can be written as Equation (20) and (21) respectively.

$$Y(s) = \left[\frac{C_1^2(s)G_1(s)G_{In}}{1 + C_1(s)G_{In} + C_1^2(s)G_1(s)G_{In}}\right] ACE_i - \left[\frac{G_1(s)}{1 + C_1(s)G_{In} + C_1^2(s)G_1(s)G_{In}}\right] \Delta P_{Di} \tag{20}$$

$$G_{In} = G_{2T}(s) + G_{2H}(s) + G_{2W}(s) + G_{2G}(s) \tag{21}$$

3.3. Benefits of the proposed controller structure

This part of the work discusses a multi-non-conventional source system with thermal, hydro, wind, solar, and gas sources considered. Dash et al. [10, 11] demonstrated that the cascaded controller can effectively steady 3-area/4-area systems. Since a total of five sources are implemented in each area, the cascaded controller is selected to regulate the system. The basic controller configuration was altered to decrease the overall quantity of controllers and the control parameters, as the bulky dimensions of the system would require a enormous number of controllers.

Operation of the cascaded controller is based on the idea of distributing the regulatory mechanism between the primary and secondary loops, which improves the steadiness and response time of the system. Thus, to implement the idea in a complex multi-non-conventional system, it is divided into two parts (i.e., inner and outer part). Here, the inner controller (PID) monitors the individual sources and the outer PID controller monitors the entire area. Thus, a total of 10 PID controllers are required to regulate the entire system, as shown in Fig. 1b, instead of a total of 16 controllers as per the traditional cascaded design presented in Fig. 2b. This enhances the cost-effectiveness of the proposed C-PID controller in the system. The installation of an optimal set of controllers will reduce any undesirable delay in initiating a regulatory action. Considering the modern power scenario in which generation through non-conventional source is considered to be economical as well as essential, the proposed controller structure would further boost the economy of the system and would simultaneously maintain the reliability and stability of the system.

4. Objective function formulation

To find a better solution to the optimization problem, formulation of the objective function is essential. The optimization module is significantly influenced by the selected objective function, which may be an integral of time multiplied by absolute of error (*ITAE*), an integral of time with squared error (*ITSE*), an integral squared error (*ISE*), or an integral of absolute error (*IAE*). Traditionally, either *ITAE* or *ITSE* is selected as the objective function, based on their ability to curb the transient error by highly penalizing the cause, which improves the steady state response. However, with the classic features of reduction of overshoot and number of oscillations, the Integral of Squared Time and Squared Error (*ISTSE*) [33] function is employed as an objective function in this study and was tested under a varying load scenario. The settling time following a disturbance is effectively controlled by the *ITAE* criterion, as it gives higher significance to the absolute of the overall error value, which pushes the response faster towards zero in a minimization case. Any controller tuned with the help of the ITSE function tends to generate larger regulatory signals, which is highly dangerous in scenarios of sudden change in load-generation balance or successive system failure, as it directs the system to higher degrees of quasi-stable states. Smaller weights are assigned to load imbalances with greater magnitude but the errors that occur late are heavily penalized in the *ITAE* function. Furthermore, the additional weight added to the time parameter ensures faster settling of the studied dynamic system. Thus, *ISTSE*, which has the advantages of both *ITAE* and *ITSE*, is a clear selection [34]. The formulation of objective function is depicted in Equation (22).

$$ISTSE = \int_0^{t_{sim}} (|\Delta F_1| + |\Delta F_2| + |\Delta P_{tie}|)^2 . t^2 . \mathrm{d}t \tag{22}$$

ΔF_1 and ΔF_2 are the fluctuation in frequency in area-1 and 2, respectively, whereas ΔP_{tie} represents the change in power in the tie line. The summation of ΔF_1, ΔF_2, and ΔP_{tie} is the total error product of the system that is used for the calculation of *ISTSE* function. The performance of *ISTSE* was evaluated by conducting experimental analysis on the model and results were compared to other popular objective function, including Integral Time Absolute Error

Table 1
Objective function comparison

Objective function	Under Shoot ($\times 10^{-3}$)	Peak Time	Settling Time	Objective Function Value
ITSE	5.85	0.5827	11.16	1.0715
ITAE	5.71	0.5849	12.19	1.0381
ISTSE	**2.84**	**0.5765**	**10.53**	**0.8741**

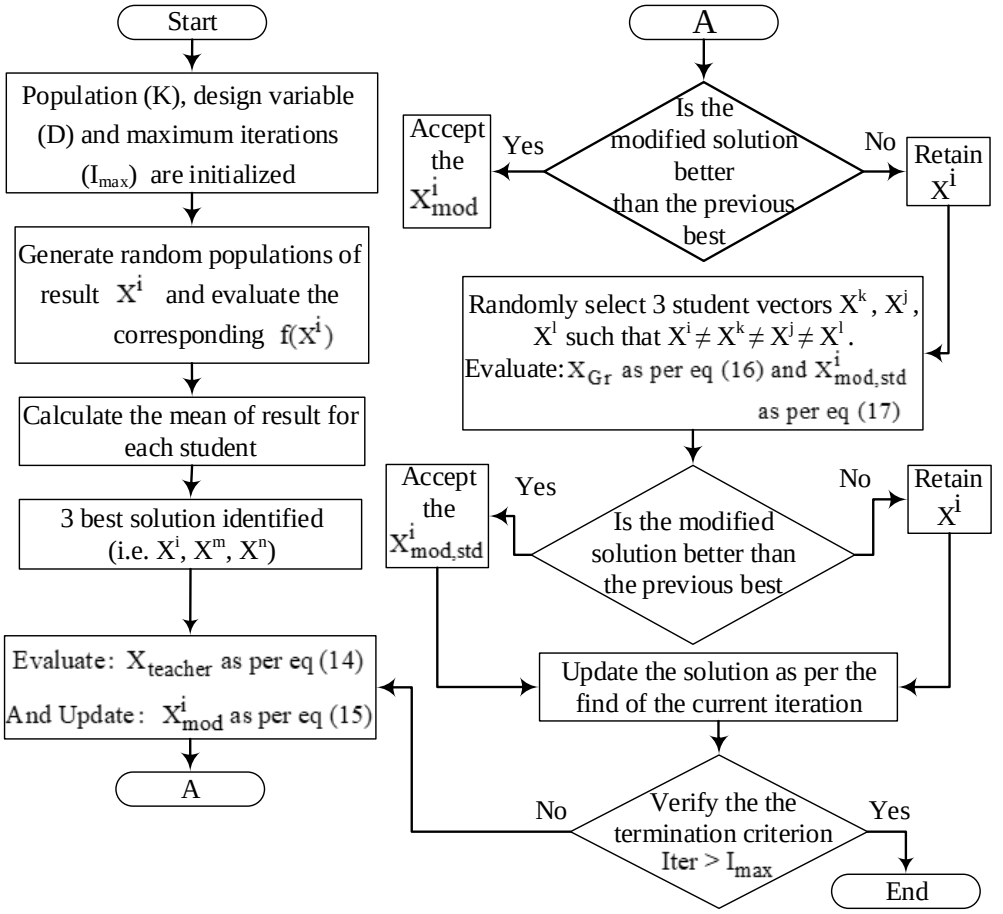

Figure 3: Flow chart of the hITLBO-DE technique.

(*ITAE*) and Integral Time Squared Error (*ITSE*) as in Table-1. Here, *ISTSE* shows the least objective function value and better performance in terms of Under Shoot, Peak Time and Settling Time. In Table-1, Under Shoot is the maximum deviation in frequency, Peak Time is the time required to reach the first peak post disturbance, Settling Time is the time required for the response to reach $\pm 2\%$ of peak value, and the Objective Function Value is evaluated as per Equation (22).

5. Optimization technique

An optimization technique is essential to the entire process of maintaining system stability. The considered dynamic turbine system responds to the change in loading. In a large power system that has numerous controllers, it is difficult to manually find an optimum controller setting. Thus, in the study, a hybrid optimization technique is proposed that is

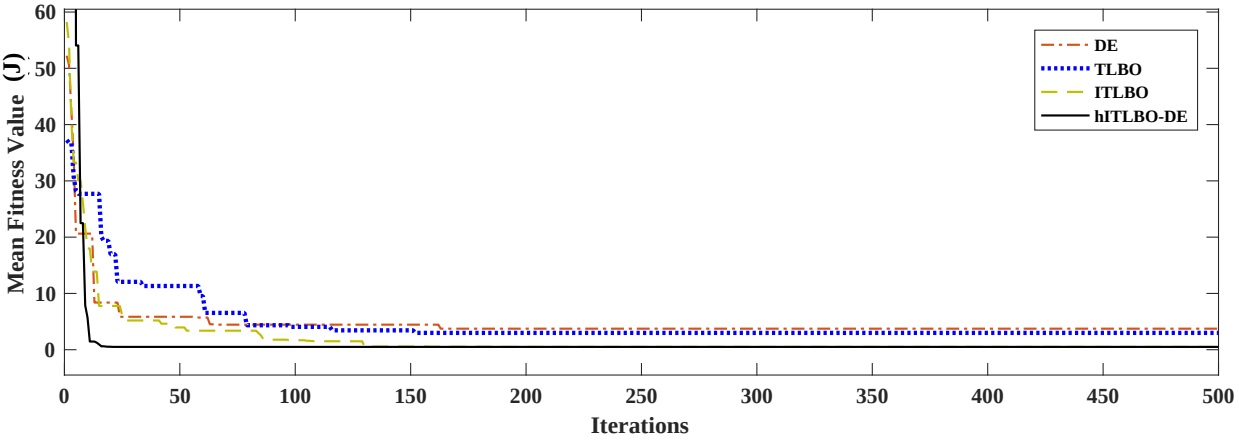

Figure 4: Convergence graph for various optimization techniques applied to the multi-source power system.

a combination of Differential Evolution (DE) [35, 36] and Teaching Learning Based Optimization (TLBO) [8, 9]. By focusing on the local and self-learning process of TLBO, Chen et al. [37] modified the basic structure of TLBO and proposed an improved ITLBO. The combination of effective DE along with the result of the oriented ITLBO algorithm provides a road map for enhanced optimization capabilities in a tuning process. The ITLBO algorithm comprises of two phases (i.e. teacher and student phase), for the obtaining the optimized parameter values. Due to limited learning abilities, the student learns from neighbouring students. The concept of mutual learning is enhanced by the proposal of group learning for students. Here, the mutation phase of DE is implemented to the learning process of both the teacher and student phase. A flowchart of the proposed hITLBO-DE technique is shown in Fig.3. Productivity analysis of this technique is performed by applying the technique to various benchmark test functions. Un-constrained and constrained benchmark functions are solved by the proposed optimization technique and the results are presented in Table-2, 3. The following section briefly describes the hybrid optimization technique.

5.1. Brief report on hITLBO-DE

The newly developed algorithm was formulated by using DE in the teacher and student phase of the ITLBO method. The primary stage is the teacher phase that is a greatly influential phase for the improvement in student response as well as the self-learning ability of the student. The prime objective of the teacher solution is to guide the student solutions away from local minima. Hence, the concept of mutation process of DE is executed in the ITLBO at both the teaching learning stage and student self-learning stage. The mathematical representation of formulation of the hybrid technique is depicted in Equations (23) to (26); this is also addressed in the flowchart in Fig. 3 for the purpose of better understanding. Equations (23) and (24) are used to revise $X_{teacher}$ in the teacher phase as per the layout of the hybrid technique. Values for each student solution (X^i_{mod}) is attained through interaction with $X_{teacher}$, as per Equation (23). Here, T^i_f, the teacher factor, must be within a closed interval [1, 2] and $T^i_f \in \mathbb{N}$. Furthermore, X^i_{mod} is evaluated for each of the i^{th} iterations and X_{mean} is the mean of each student over all the iterations.

$$X_{teacher} = X^i + M(X^m - X^n) \tag{23}$$

$$X^i_{mod} = X^i + rand(0, 1)[X_{teacher} - (T^i_f \times X_{mean})] \tag{24}$$

Here, $X_{teacher}$, which is an essential element for student progress, is evaluated by incorporating the mutation state of DE to the student phase through the mutation factor $'M'$. In the proposed methodology, the three best solutions (X_i, X_m and X_n) are selected and are used to improve the results of the teacher vector in the self-adaptive phase, as in Equation (23). Moreover, these combinations of solutions enhance the ability of the teacher to isolate the global best solution and better tutoring of student vector. A similar application in the student phase enables the students to learn from neighboring student in a group (many-to-one learning) instead of the traditional concept of one-to-one learning. Equations (25) and (26) are formulated to execute these steps. Hence, three students were identified randomly such that

Table 2
Performance testing of proposed hITLBO-DE with unconstrained benchmark functions.

Single objective optimization						
Function name	Test function	Range	Optimization technique	Best	Worst	Mean
Ackely	$F_1(x,y) = -20exp(-0.2\sqrt{\frac{1}{n}\sum_{i=1}^{n} x_i^2})$	$[-32,32]^n$	ITLBO	1.092×10^{-13}	1.421×10^{-11}	1.263×10^{-12}
			DE	4.508×10^{-12}	1.984×10^{-11}	7.436×10^{-12}
			hITLBO-DE	4.440×10^{-15}	1.090×10^{-12}	1.354×10^{-13}
Beale	$F_2(x,y) = \sum_{i=1}^{n}(ix_i)^4 + random(0,1)$	$[-4.5,4.5]^n$	ITLBO	0.571	1.923	1.057
			DE	1.204	1.549	1.507
			hITLBO-DE	1.135×10^{-9}	1.734	1.382×10^{-3}
Booth	$F_3(x,y) = (x+2y-7)^2 + (2x+y-5)^2$	$[-10,10]^n$	ITLBO	0.168×10^{-7}	0.803×10^{-5}	0.483×10^{-6}
			DE	0.799×10^{-7}	0.159×10^{-4}	0.807×10^{-6}
			hITLBO-DE	0.519×10^{-25}	0.479×10^{-5}	0.192×10^{-8}
Goldstein-Price	$F_4(x,y) = [1+(x+y+1)^2(19-4x+3x^2 -4y+6xy+3y^2)][30+(2x-3y)^2 (18-32x+12x^2+48y-36xy+27y^2)]$	$[-2,2]^n$	ITLBO	3.00	11	5.492
			DE	3.00	22	5.329
			hITLBO-DE	3.00	8	3.461
Levi N.13	$F_5(x,y) = \sin^2 3\pi x + (x-1)^2 (1+\sin^2 3\pi y) + (y-1)^2(1+\sin^2 2\pi y)$	$[-10,10]^n$	ITLBO	1.736×10^{-6}	1.642	0.098
			DE	1.097×10^{-5}	0.674	0.086
			hITLBO-DE	1.7061×10^{-31}	$0.735\ 1.298\times10^{-3}$	
Noisy quadric	$F_6(x) = \sum_{i=1}^{n}(ix_i)^4 + random(0,1)$	$[-1.2,1.2]^n$	ITLBO	0.156	1.170	0.324
			DE	0.885	1.588	1.094
			hITLBO-DE	0.213	1.834	0.624
Rastrigin	$F_7(x) = \sum_{i=1}^{n}(x_i^2 - 10\cos 2\pi x_i) +150$	$[-5.1,5.1]^n$	ITLBO	2.842×10^{-14}	8.547	1.605
			DE	8.529×10^{-13}	4.292	1.229
			hITLBO-DE	2.842×10^{-4}	6.186	3.055
Rosenbrock	$F_8(x) = \sum_{i=1}^{n-1}(100(x_{i+1}-x_i^2)^2$	$[-30,30]^n$	ITLBO	8.793×10^{-6}	9.873×10^{-5}	3.175×10^{-5}
			DE	5.462×10^{-5}	1.691×10^{-4}	4.304×10^{-5}
			hITLBO-DE	4.250×10^{-6}	7.472×10^{-5}	3.075×10^{-5}
Schwefel	$F_9(x) = max(\lvert x_i\rvert, 1\le i\le n)$	$[-100,100]^n$	ITLBO	3.575×10^{-10}	1.722	0.998
			DE	6.771×10^{-10}	2.037	1.008
			hITLBO-DE	3.575×10^{-13}	1.722×10^{-11}	2.048×10^{-11}
Sphere	$F_{10}(x) = \sum_{i=1}^{n}(x_i^2)$	$[-100,100]^n$	ITLBO	6.771×10^{-13}	7.943×10^{-11}	2.699×10^{-11}
			DE	4.295×10^{-12}	8.689×10^{-11}	2.937×10^{-11}
			hITLBO-DE	5.960×10^{-40}	5.308×10^{-36}	5.773×10^{-37}
Step	$F_{11}(x) = \sum_{i=1}^{n}(x_i+0.5)^2$	$[-100,100]^n$	ITLBO	0.946×10^{-35}	0.938×10^{-31}	1.651×10^{-33}
			DE	0.703×10^{-30}	0.023×10^{-26}	1.076×10^{-28}
			hITLBO-DE	1.661×10^{-5}	0.674	1.992

$X_i \neq X_k \neq X_j \neq X_l$, where X_i denotes the student vector. These students use their self-learning skills to reach the global solution as a whole in this many-to-one process. The hybrid hITLBO-DE algorithm retains the characteristics of not getting trapped by local minimal in the mutation operation as it is manipulated by the group learning ability of the three variables simultaneously. Thus, it rapidly converges to a global minimum while operating reliably.

$$X_{Gr} = X_j + M(X_k - X_l) \tag{25}$$

Table 3
Performance testing of proposed hITLBO-DE with constrained benchmark functions.

Constrained optimization					
Function name	Test function and Constraints	Optimization Technique	Best	Worst	Mean
Mishra's Bird	$F_{11}(x,y) = \sin(y)e^{(1-\cos x)^2} + \cos(x)e^{(1-\sin y)^2+(x-y)^2},$	ITLBO	-106.219	-89.280	-106.415
	Subjected to:	DE	-106.693	-97.303	-106.723
	$(x+5)^2 + (y+5)^2 < 25$	hITLBO-DE	-106.764	-106.394	-106.764
Rosenbrock (cubic)	$F_{12}(x,y) = (1-x)^2 + 100(y-x^2)^2,$	ITLBO	1.661×10^{-7}	2.926	0.834
	Subjected to:	DE	1.729×10^{-6}	0.910	0.519
	$(x-1)^3 - y + 1 < 0$ and $x + y - 2 < 0$	hITLBO-DE	8.161×10^{-11}	0.958	0.318
Rosenbrock (disk)	$F_{13}(x,y) = (1-x)^2 + 100(y-x^2)^2,$	ITLBO	2.518×10^{-7}	2.115	0.209
	Subjected to:	DE	1.748×10^{-6}	1.225	0.837
	$x^2 + y^2 < 2$	hITLBO-DE	2.627×10^{-15}	0.239	0.031
Simionescu	$F_{14}(x,y) = 0.1xy,$	ITLBO	-0.0720	-0.0621	-0.0710
	Subjected to:	DE	-0.0722	-0.692	-0.0718
	$x^2 + y^2 \leq [r_t + r_s\cos(n\arctan\frac{x}{y})]^2$	hITLBO-DE	-0.0726	-0.0719	-0.0720
Townsend	$F_{15}(x,y) = -[\cos((x-0.1)y)]^2 - x\sin(3x+y),$	ITLBO	-2.0221	-1.689	-1.655
	Subjected to:	DE	-1.6595	-1.676	-1.689
	$x^2 + y^2 < [2\cos t - \frac{1}{2}\cos 2t - \frac{1}{4}\cos 3t - \frac{1}{8}\cos 4t]^2 + [2\sin t]^2$	hITLBO-DE	-2.0231	-1.639	-1.931

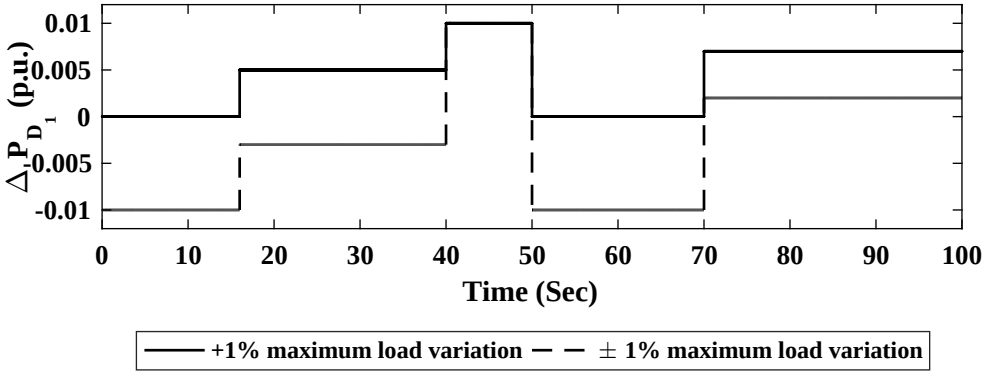

Figure 5: Dynamic load variation applied to the tested system.

$$X^i_{mod,std} = X^i + rand(0,1)[X^i - X_{Gr}] \tag{26}$$

Thus, a rapid convergence is observed as the optimal result is reached in lower number of iterations and execution time. The developed optimization methodology is initially subjected to standard benchmark functions, as shown in Table-2 and Table-3, respectively, and was then applied to the 2-area dynamic turbine thermal system. The minimum value of the unconstrained benchmark functions F_1 to F_3 and F_5 to F_{11} is 0, whereas the minimum value of F_4 is 3. Minimum values for constrained functions F_{12}- F_{16} are -106.764, 0, 0, -0.072 and -2.023 respectively.

6. Performance and stability analysis of the 2-area multi-non-conventional source system

In this section, stability analysis was initially performed to project the steadiness of the system under varying loads. Next, the performance of the system was tested by application of step load changes that were discussed in Case-I, II, III, and IV and a dynamically varying load for 100 seconds as discussed in Case-V, VI, and VII. Here, the proposed controller that was tuned by the hITLBO-DE technique is used to keep the system in a stable zone of operation. Numerous ranges of outer loop parameters (K_{Po}, K_{Io}, K_{Do}) were purposefully verified (i.e., [-2, 2], [0, 2], [0, 3], [0, 4], [0, 5]). And range of [0, 5] was found as a suitable range. The range [0, 2] has been expansively used in several

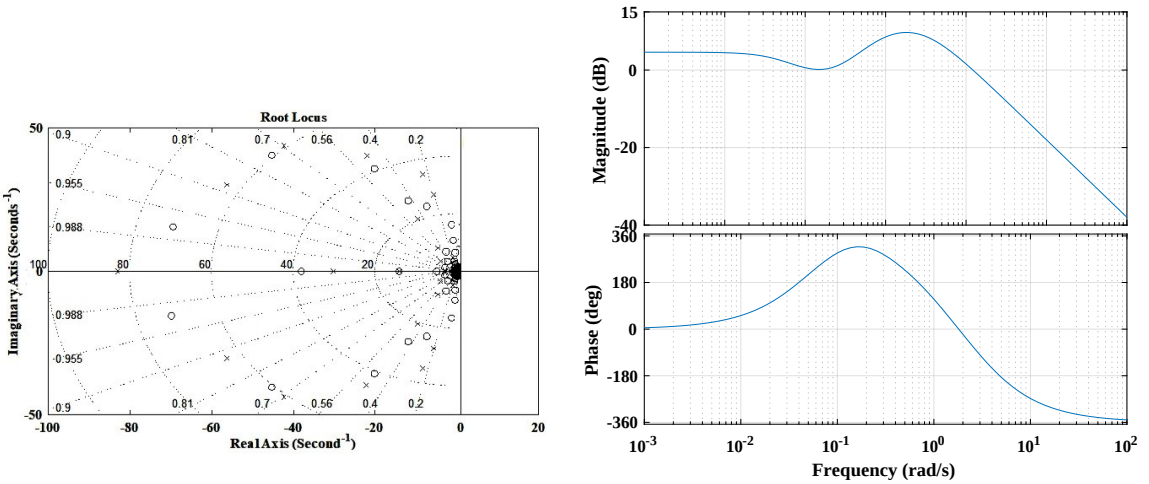

Figure 6: (a) Root locus analysis, (b) Bode plot analysis for the 2-area multi-non-conventional system.

publications, where traditional [6, 38, 10, 11] and non-conventional [39, 9] sources are typically studied. However, in [29], the dynamic model of wind and diesel was projected and it is concluded that any non-liner modelling would require relatively greater values of controller parameters. In [29], $K_P = 10.0$ and $K_I = 4.0$ was used to sustain a steady operation with wind and diesel generation plants. Here, the outer controller regulates the entire area (i.e., dynamic steam turbine, hydel, wind, solar, and gas sources) as one system; hence, a higher value of the specified parameters is required. Therefore, the parameters for the designed controller configuration tuned by the proposed hITLBO-DE algorithm have their boundary condition defined as $0 \leq K_{Pi},\ K_{Ii},\ K_{Di} \leq 2.0$ and $0 \leq K_{Po},\ K_{Io},\ K_{Do} \leq 5.0$.

The proposed modified C-PID controller was incorporated into the considered system in a MATLAB environment, and the evaluation was made for different cases. Here, a 1% step load change in area-1 only is Case-I, a 1% step load change in both area-1 and area-2 is Case-II, a 5% step load change in both area-1 and area-2 is Case-III, and a 10% step load change in both area-1 and area-2 is Case-IV.

As shown in Fig. 5, Case-V has a maximum load variation of 1% with individual variation of +0.5% at t= 16s, +0.5% at t= 40s, -1% at t= 50s, +0.7% at t= 70s is applied to area-1 only, for Case-VI same load variation as in Case-V is applied but to both area-1 and area-2 and Case-VII has maximum load variation of ± 1% with individual variation being -1% at t = 0s, +0.7% at t = 16s, +1.3% at t = 40s, -2% at t = 50s, +1.2% at t = 70s.

6.1. System stability analysis

For a given system, stability under varying operating conditions is essential in order to satisfy the major objective of a power system. The root-locus, bode plot, and eigenvalue analysis was conducted on the 2-area multi-non-conventional source system to study the system stability after implementation of the formulated C-PID controller. Fig. 6a shows the plot of the roots of the characteristics equation describing the power system. From this analysis, it can be seen that there are a significant number of dominant poles that drives the system toward enhanced stability. It can be observed in Fig. 6b that the bode plot is quite smooth for even the increased complexity due to integration of various non-conventional sources. Finally, eigenvalue analysis was performed and the frequency of oscillation and the damping ratio were evaluated, Table-4.

The power system is majorly affected by any external fault, system outages, or imbalances in generation-load as per Equation (27).

$$\Delta P_G = \Delta P_l + \Delta P_D \tag{27}$$

Here, ΔP_G, ΔP_l, ΔP_D are the deviation in generated power, power lost during transmission, and demand power, respectively. A close loop nonlinear system is presented by Equation (28) and the approximate linear system can be written as shown in Equation (29). The system has been linearized around the operating point ω_0 and δ_0, which represents the frequency and tie-line power prior to any fault occurrence.

$$\dot{X} = f(\omega, \delta) \tag{28}$$

Table 4
Eigen value analysis of the 2-area multi-non-conventional system.

Modes	Eigen value	Freq. of oscillation	Damping ratio
λ_1, λ_4	-0.02	-	1
λ_2, λ_5	-0.001	-	1
λ_3, λ_6	-0.0002	-	1
λ_7, λ_8	-4.391	-	1
λ_9	-0.243	-	1
λ_{10}	-0.1995	0.0058	0.1699
λ_{11}	-0.1993	-	1
λ_{12}	-0.1232	-	1
λ_{13}	-0.1203	-	1
λ_{14}, λ_{15}	-0.0275±j0.0305	4.790	0.6696
λ_{16}, λ_{17}	-0.0401±j0.0117	1.8370	0.9599
λ_{18}	-0.0430	-	1
λ_{19}	-0.0432	-	1
λ_{20}, λ_{21}	-0.0329±j0.0050	0.7853	0.9886
λ_{22}	-0.0232	-	1
λ_{23}, λ_{24}	-0.0014±j0.0017	0.2670	0.6357
λ_{25}, λ_{26}	-0.0003±j0.0007	0.1099	0.3939
λ_{27}	-0.0016	-	1
λ_{28}	-0.0018	-	1
λ_{29}, λ_{30}	-0.0095±j0.0013	0.2042	0.9907
λ_{31}	-0.0102	-	1
λ_{32}, λ_{33}, λ_{34}	-0.01	-	1
λ_{35}, λ_{36}	-0.0003±j0.0005	0.0785	0.5144
λ_{37}	-0.2439	-	1
λ_{38}, λ_{39}	0	-	-

$$\dot{X} = A\omega + B\delta; \quad \omega, \delta \in \mathbb{R}^{\mathrm{m}} \text{ and } \mathrm{A}, \mathrm{B} \in \mathbb{R}^{\mathrm{m}\times\mathrm{m}} \tag{29}$$

If A and B matrices are non-singular matrices, then the system that is defined by Equation (29) is at equilibrium only at the origin.

Thus, stability analysis of the system can be done considering the following statements.

(a) If all the eigenvalues have a negative real part then the considered model is said to be asymptotically stable.

(b) If the eigenvalues have a negative real part, at least one eigenvalue is present with zero as the real part and $D_\lambda = M_\lambda$ for every eigenvalue with zero real part. D_λ is the geometric multiplicity and M_λ is the algebraic multiplicity for each eigenvalue.

(c) If (a) is not satisfied and there is any eigenvalue with zero real part for which $D_\lambda < M_\lambda$; then the system must be unstable.

The algebraic multiplicity is the maximum number of occurrences for a particular eigenvalue and geometric multiplicity is a dimension of nullity found for the matrix $(A - \lambda I)$. Table-4 shows that all eigenvalues have a negative real part and the last eigenvalue has a zero real part with $D_\lambda = M_\lambda$. Hence, it is concluded that the system is stable under varying operating conditions.

Table 5
Parameters of various controller tuned by hITLBO-DE technique for the 2-area multi-non-conventional system.

	Controller type	Optimization technique	Power Source	Inner loop controller			Outer loop controller		
				K_{Pi}	K_{Ii}	K_{Di}	K_{Po}	K_{Io}	K_{Do}
Area-1 controllers	I	hITLBO-DE	Thermal	-	1.0736	-	-	-	-
			Hydro	-	1.5468	-	-	-	-
			Wind	-	1.8441	-	-	-	-
			Gas	-	1.0090	-	-	-	-
	PI	hITLBO-DE	Thermal	1.4340	1.1996	-	-	-	-
			Hydro	0.4276	0.0595	-	-	-	-
			Wind	1.5290	1.3801	-	-	-	-
			Gas	1.7734	0.6349	-	-	-	-
	PID	hITLBO-DE	Thermal	1.3470	1.2339	1.6856	-	-	-
			Hydro	1.3124	1.0051	0.6166	-	-	-
			Wind	1.1793	1.5669	1.5317	-	-	-
			Gas	0.3798	1.3985	0.1461	-	-	-
	C-PID	ITLBO	Thermal	1.1618	1.5425	1.9714	2.3925	4.0881	2.4430
			Hydro	0.8109	1.6443	1.1998			
			Wind	1.2755	0.4877	1.5539			
			Gas	0.9195	0.8131	3.6517			
	C-PID	DE	Thermal	1.7344	1.4918	1.8930	4.7987	4.7875	3.9742
			Hydro	1.0863	1.6427	1.7019			
			Wind	1.5561	0.2483	1.1864			
			Gas	0.5950	1.8926	0.8282			
	C-PID	hITLBO-DE	Thermal	2.6540	1.4834	1.4488	4.5136	3.2216	4.8244
			Hydro	0.9344	1.5236	0.4056			
			Wind	1.2652	0.8958	1.5939			
			Gas	1.9011	1.1103	1.0493			
Area-2 controllers	I	hITLBO-DE	Thermal	-	1.4543	-	-	-	-
			Hydro	-	1.3149	-	-	-	-
			Wind	-	1.9263	-	-	-	-
			Gas	-	0.7881	-	-	-	-
	PI	hITLBO-DE	Thermal	1.1191	1.6886	-	-	-	-
			Hydro	1.4463	1.7536	-	-	-	-
			Wind	1.6641	0.6057	-	-	-	-
			Gas	0.7340	1.4461	-	-	-	-
	PID	hITLBO-DE	Thermal	1.4269	1.6950	1.4954	-	-	-
			Hydro	1.2755	1.1580	0.4191	-	-	-
			Wind	1.7408	0.7094	0.5560	-	-	-
			Gas	1.5003	1.7508	1.1203	-	-	-
	C-PID	ITLBO	Thermal	0.1786	1.1524	1.9807	3.0099	2.2942	4.7239
			Hydro	1.2875	1.4258	0.6599			
			Wind	1.9807	0.1786	1.1524			
			Gas	0.6599	1.2875	1.4258			
	C-PID	DE	Thermal	1.3664	0.9241	1.3846	4.0579	4.8530	3.2704
			Hydro	1.9989	1.2688	1.7583			
			Wind	0.8450	1.2994	1.5244			
			Gas	0.1592	1.2456	1.4709			
	C-PID	hITLBO-DE	Thermal	1.5855	1.4292	1.3190	4.8154	3.7563	4.7858
			Hydro	1.4816	0.1722	1.7686			
			Wind	1.0436	0.6803	1.3111			
			Gas	1.6708	0.9448	0.9890			

6.2. System performance analysis

The proposed controller configuration was implemented in the multi-non-conventional 2-area system. The C-PID controller parameters tuned by the ITLBO, DE, and formulated hITLBO-DE optimization algorithm has been presented in Table-5. Also, the parameters for I, PI, and PID controller tuned by the formulated hITLBO-DE algorithm has been presented in Table-5. The performance of the system with various controllers (I, PI, PID, and C-PID) for Case-I is

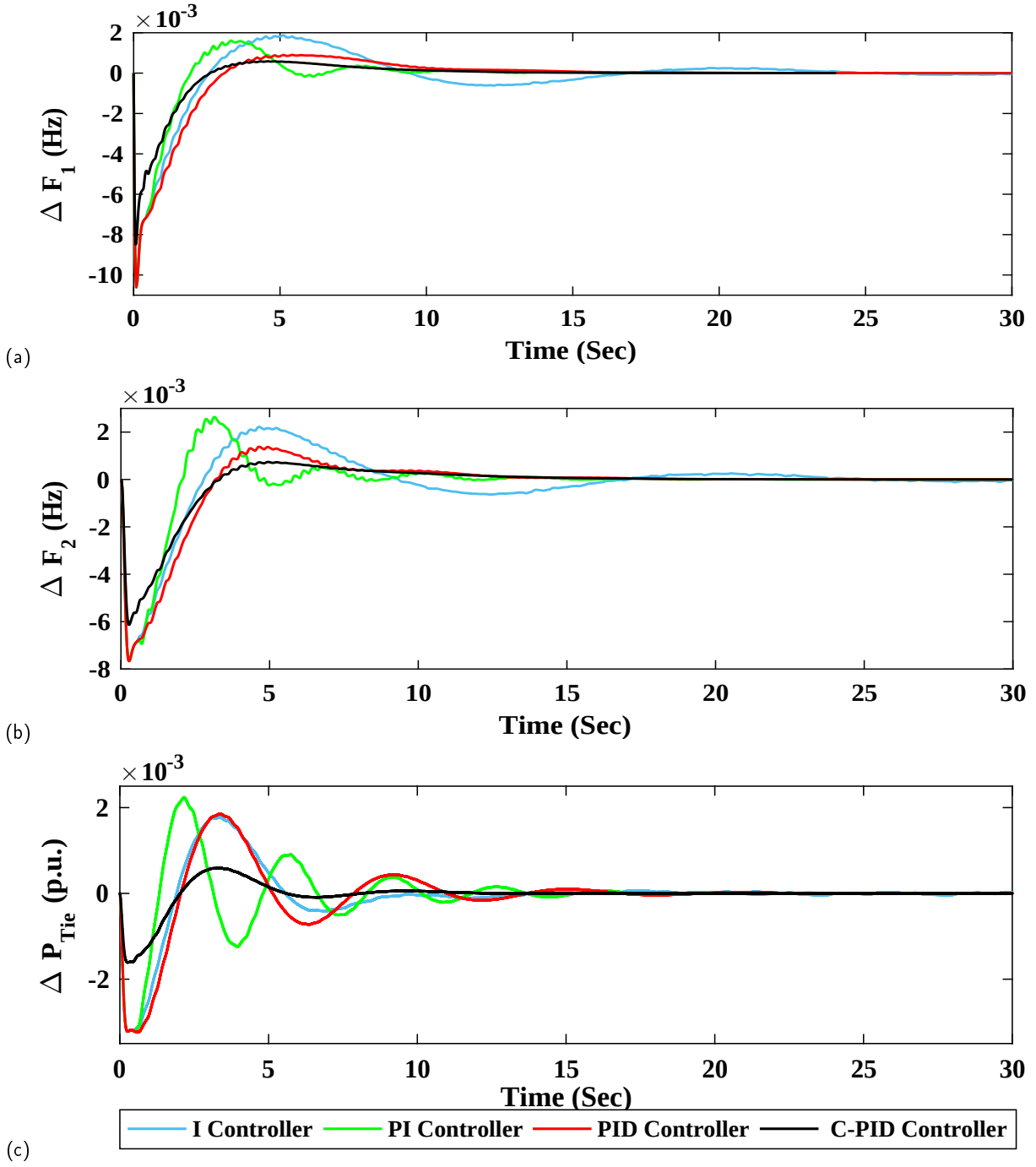

Figure 7: Deviation in (a) Frequency for area-1 (b) Frequency for area-2 (c) Tie line power for various controllers implemented to the 2-area multi-non-conventional system for Case-I.

shown in Fig. 7. From Fig. 7, it is observed that the proposed C-PID controller tuned by hITLBO-DE algorithm outperforms the other controller schemes in terms of Over/Under shoot and 2% Settling time of the system response. Fig. 8 shows the response of the system for perturbations described in Case-I, II, III, IV. Here, it is clearly observed that the formulated scheme of C-PID controller and hITLBO-DE algorithm is able to maintain the system stability after occurrence of perturbation discussed in Case-I, II, III, IV. The mathematical analysis of Over/Under shoot and 2%

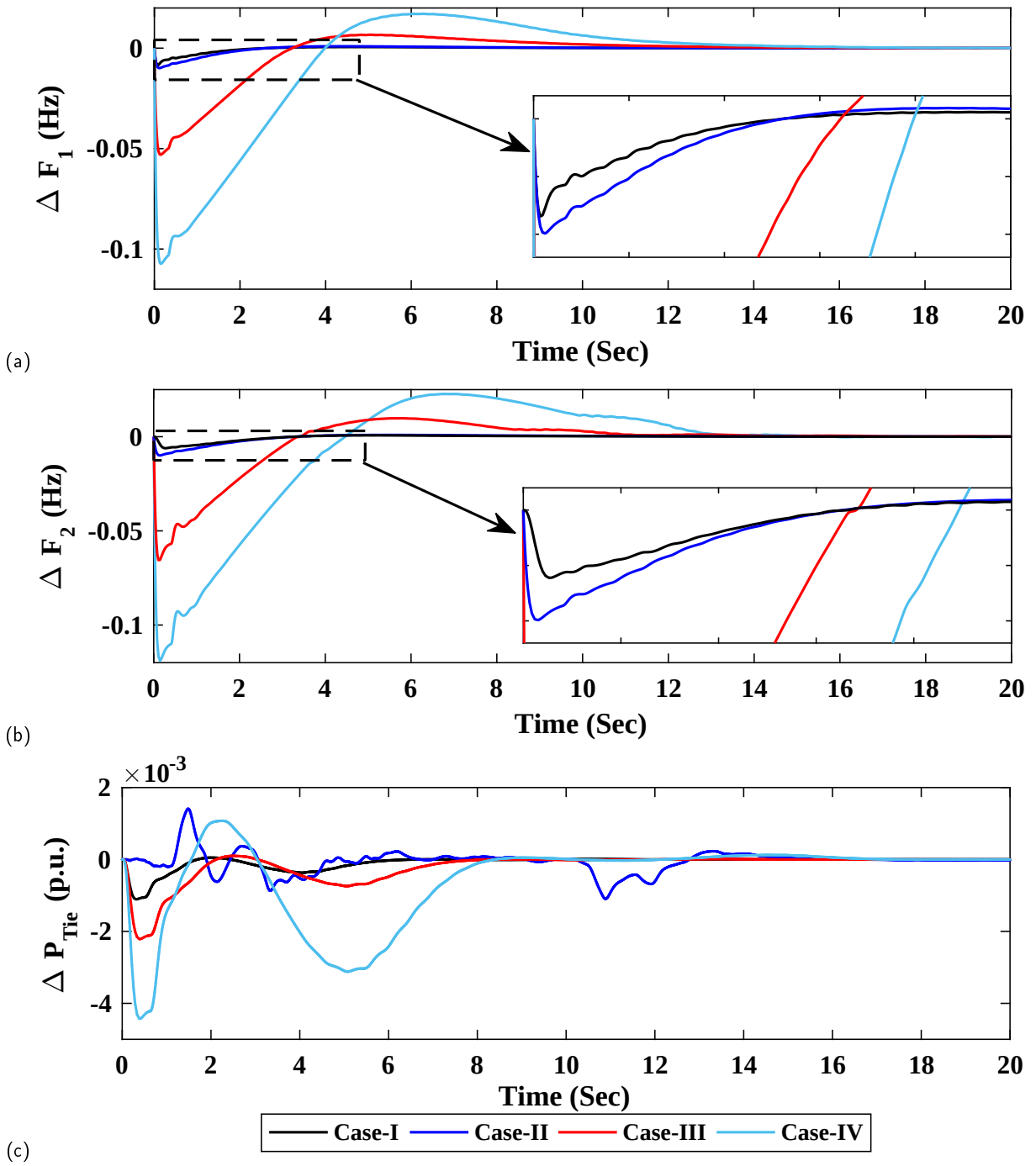

Figure 8: Deviation in (a) Frequency for area-1 (b) Frequency for area-2 (c) Tie line power for various cases of perturbation (Case-I, II, III, IV) applied to 2-area multi-non-conventional system.

Settling time of the system response presented in Fig. 7 and Fig. 8 is presented in Table-6. In Table- 6, a performance comparison of the proposed hITLBO-DE algorithm tuned I, PI, PID, and C-PID controller is presented. Fig. 9 shows the effect of RFB connected to the system (with perturbation as in Case-I), for storage of energy during low load periods when generation from the non-conventional sources is maximal. In Table- 6, the proposed C-PID controller tuned by hITLBO-DE algorithm along with the application of RFB is presented. From Fig .9 and Table- 6, it can be concluded

Table 6
Comparative analysis of system parameters for the two area multi-source system (Dynamic Turbine thermal plant and Renewable sources) with step load perturbation applied

Case/Controller		ΔF_1		ΔF_2		ΔP_{tie}	
		Over/Under shoot ($\times 10^{-3}$)	Settling time (2%)	Over/Under shoot ($\times 10^{-3}$)	Settling time (2%)	Over/Under shoot ($\times 10^{-4}$)	Settling time (2%)
Case -I	I: (hITLBO-DE)	1.833	29.22	2.214	29.72	17.78	27.95
	PI: (hITLBO-DE)	1.604	13.38	2.598	16.34	22.24	18.12
	PID: (hITLBO-DE)	0.857	15.21	1.381	16.51	18.59	16.49
	C-PID: (hITLBO-DE) Without RFB	-30.25	27.92	-32.01	28.91	-2.992	27.65
	C-PID: (hITLBO-DE) With RFB in area-1	-6.656	13.16	-13.12	17.82	-1.765	13.14
	C-PID: (hITLBO-DE) With RFB in area-2	-18.24	13.24	-18.88	18.11	-4.853	12.54
	C-PID: (hITLBO-DE) With RFB in area-1, 2	-8.484	12.97	-6.035	16.29	-1.608	12.26
Case -II	C-PID: (hITLBO-DE)	-9.930	13.28	-9.960	16.33	-0.678	15.57
Case -III	C-PID: (hITLBO-DE)	-52.64	13.67	-65.820	16.61	-3.474	14.22
Case -IV	C-PID: (hITLBO-DE)	-107.30	16.63	-118.90	16.93	-6.998	11.42

that the effect of RFB placed in area-1 is more significant than that of area-2, but the best result was obtained only when RFB was installed in both areas. Furthermore, the effect of time delay (τ) was tested, which is presented in Fig. 10. It can be clearly observed that the system was maintained in a stable region of operation by the proposed controller, even for a time delay of 4 seconds under perturbation as in Case-I.

Finally, the multi-non-conventional source system implemented with the C-PID controller tuned by hITLBO-DE algorithm was studied with three dynamic load variation cases (i.e. Case-V, VI, and VII). Response of the formulated system with perturbations as in Case-V, VI, and VII are shown in Fig. 11. It is observed that the system is able to retain its stable operation after being subjected to the perturbations discussed in Case-V, VI, and VII. Table- 7 shows the mathematical analyses in terms of Over/Under shoot and 2% Settling time for the dynamic load variation discussed in Case-V, VI, and VII.

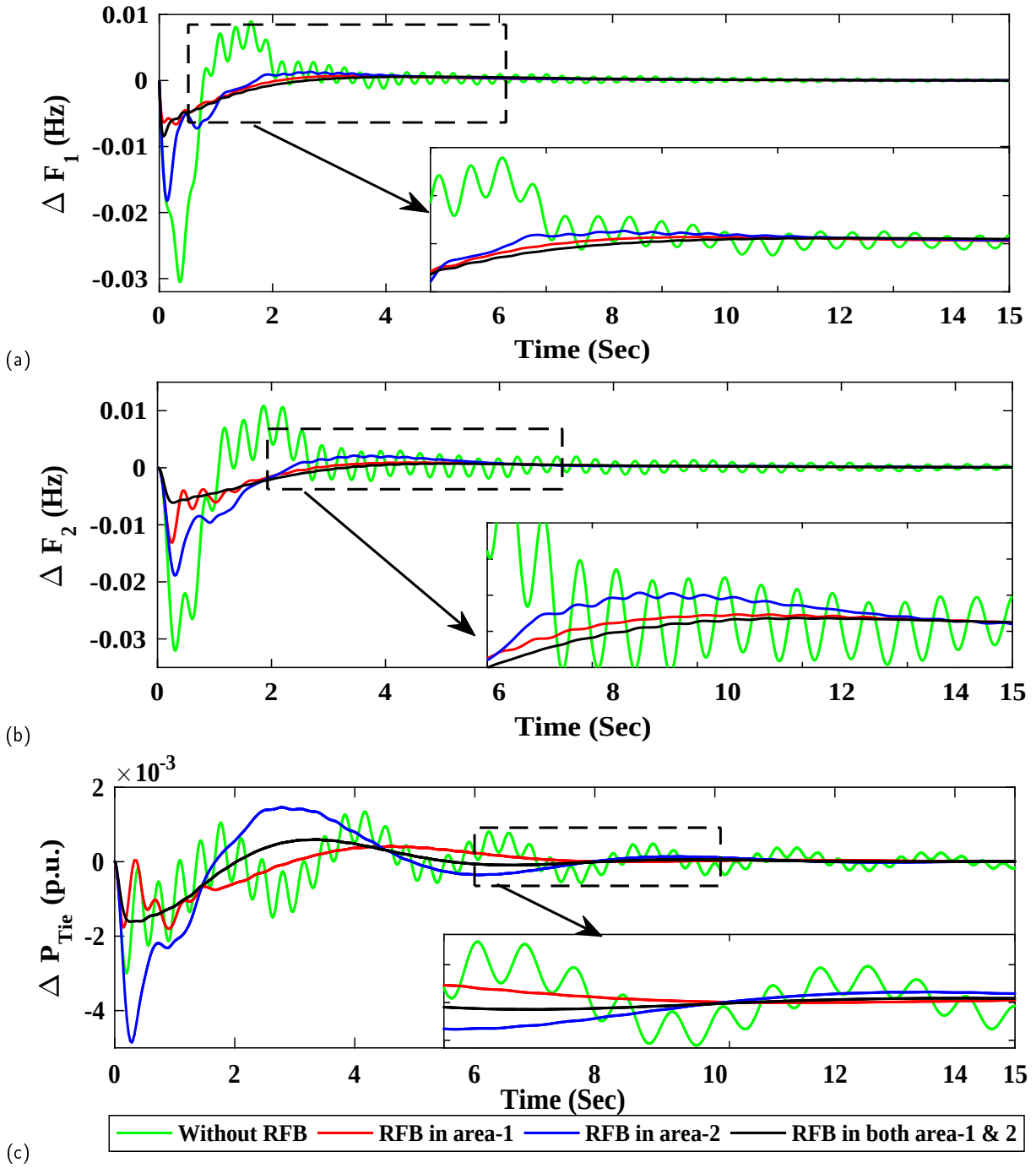

Figure 9: Deviation in (a) Frequency for area-1 (b) Frequency for area-2 (c) Tie line power for various combination of RFB connection integrated with 2-area multi-non-conventional system.

6.3. Comparison with the State-of-the-Art

For performing a comparative State-of-the-Art analysis Amelioration(%) is evaluated, as in Equation (30) and (31). AP_1, AP_2, and AP_3 represent the Amelioration(%), which indicates the percentage improvement achieved in the performance measure (i.e. Over/Under Shoot and 2% Settling time) as compared to that of the reference schemes discussed in [23] and [9]. AP_i(Under Shoot) and AP_i(Settling Time) represent the Amelioration(%) for Under Shoot

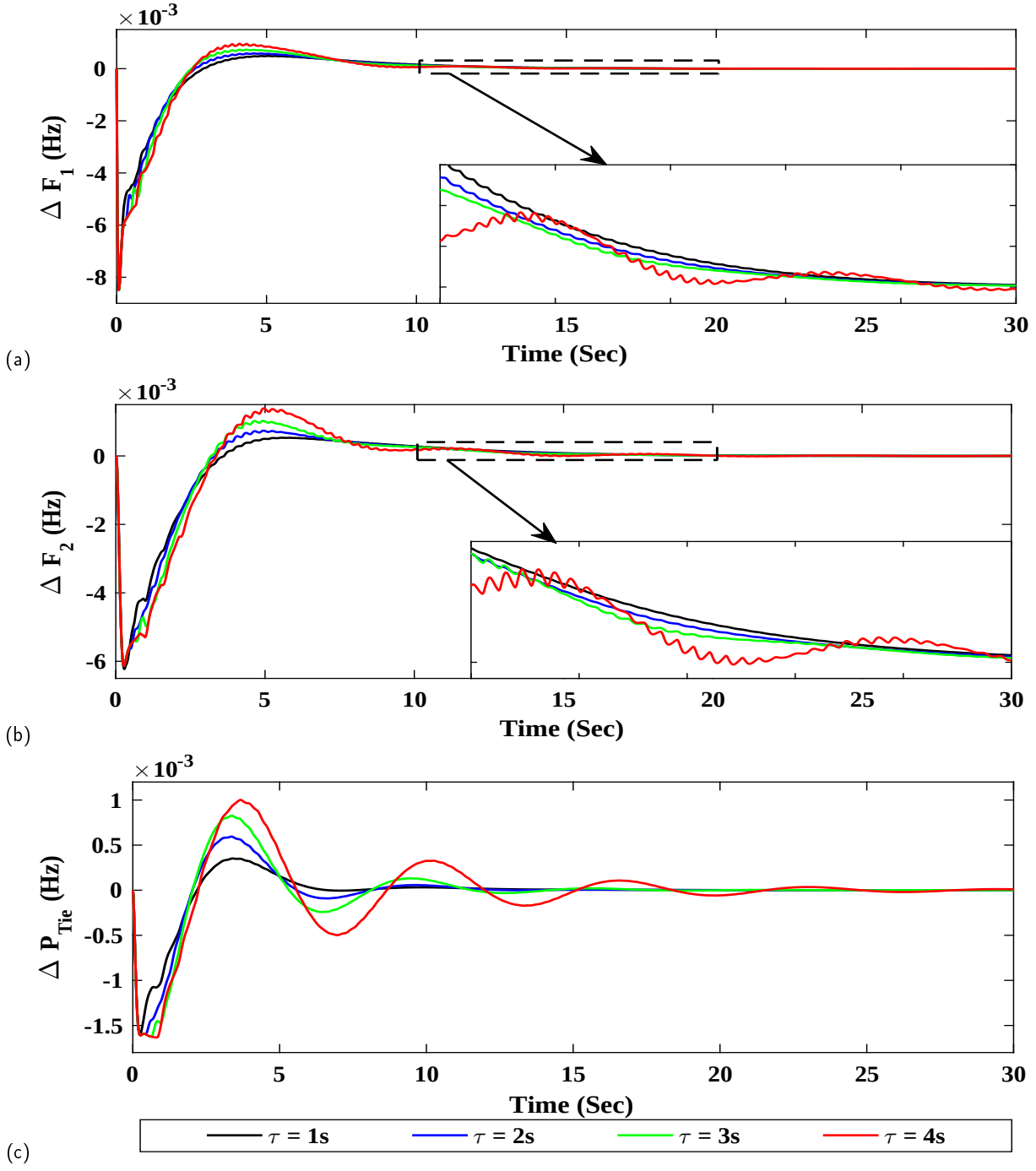

Figure 10: Deviation in (a) Frequency for area-1 (b) Frequency for area-2 (c) Tie line power for various time delay (τ) applied to 2-area multi-non-conventional system.

and Settling Time, respectively.

$$AP_i(\%)(Under\ Shoot) = \left[\frac{Under\ Shoot_{ref}}{Under\ Shoot_{obtained}}\right] \times 100 \tag{30}$$

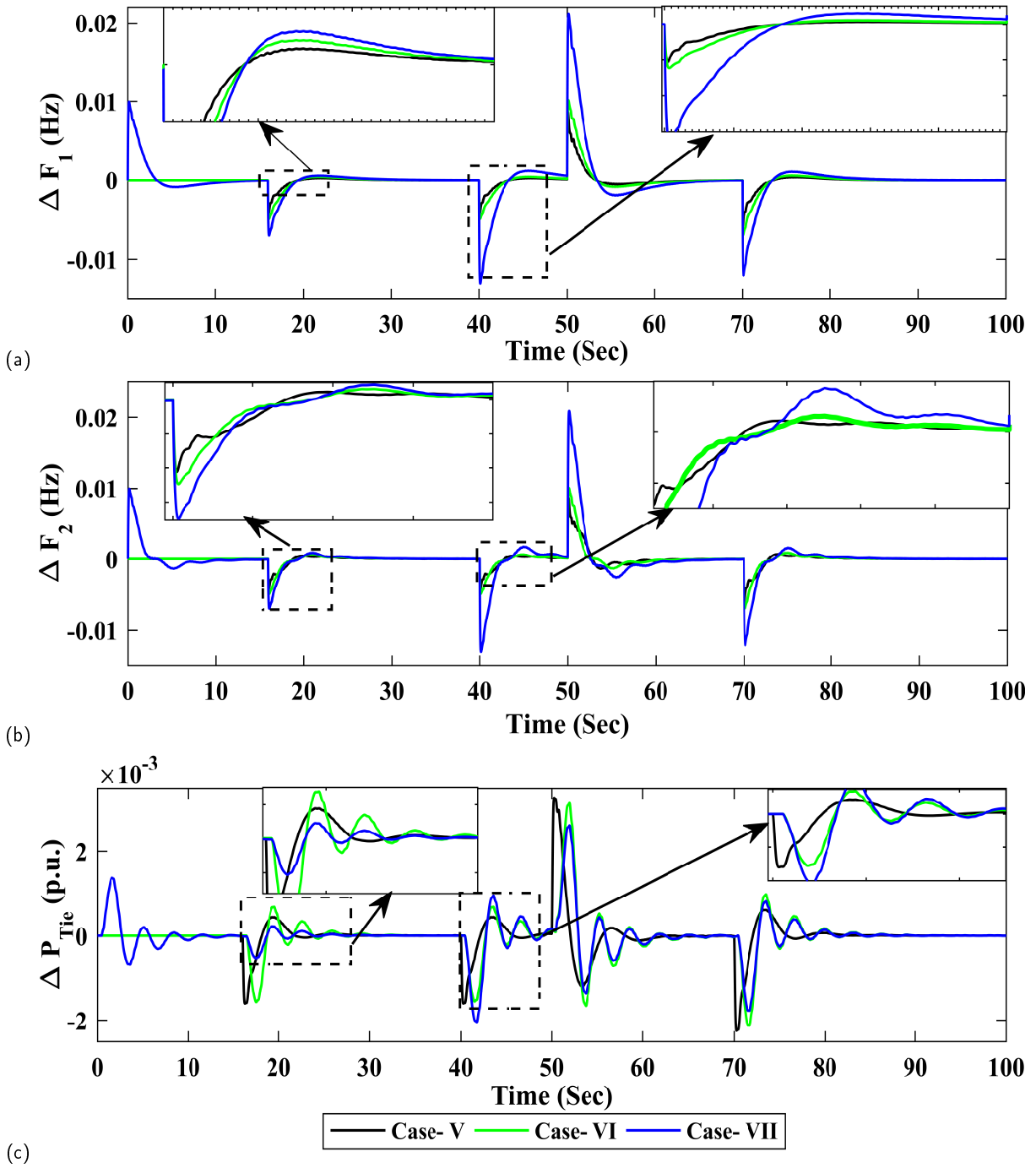

Figure 11: Deviation in (a) Frequency for area-1 (b) Frequency for area-2 (c) Tie line power for various dynamic load perturbation (Case-V, VI, VII) applied to 2-area multi-non-conventional system.

$$AP_i(\%)(SettlingTime) = \left[\frac{SettlingTime_{ref}}{SettlingTime_{obtained}}\right] \times 100 \tag{31}$$

In Table- 8, the results obtained for the proposed C-PID controller tuned by hITLBO-DE implemented in the multi-source system discussed in [23] was compared to that of a I controller tuned system in [23]. In Table- 8, $AP_1(\%)$ represents the percentage improvement in system response achieved by the proposed C-PID: hITLBO-DE when applied

Table 7
Comparative analysis of system parameters for the two area multi-source system (Dynamic Turbine thermal plant and Renewable sources) with dynamic load perturbation applied

Case/Controller			ΔF_1		ΔF_2		ΔP_{tie}	
		Various operating conditions	Over/under shoot ($\times 10^{-3}$)	Settling time (2%)	Over/under shoot ($\times 10^{-3}$)	Settling time (2%)	Over /under shoot ($\times 10^{-4}$)	Settling time (2%)
Case -V	C-PID: (hITLBO-DE)	+0.5% at t= 16 s	-4.231	27.28	-4.227	27.91	-16.02	28.20
		+0.5% at t= 40 s	-4.231	-	-4.227	-	-16.02	-
		-1% at t= 50s	8.621	62.69	8.618	62.73	32.75	62.58
		+0.7% at t= 70 s	5.934	82.67	-5.931	83.36	-22.47	82.60
Case -VI	C-PID: (hITLBO-DE)	+0.5% at t= 16 s	-4.915	27.12	-4.897	27.14	-15.28	27.97
		+0.5% at t= 40 s	-4.915	-	-4.897	-	-15.28	-
		-1% at t= 50s	10.15	62.60	10.04	63.16	31.49	65.67
		+0.7% at t= 70 s	-6.902	82.74	-6.892	83.27	-21.26	86.13
Case -VII	C-PID: (hITLBO-DE)	-1% at t= 0 s	9.95	13.76	9.950	12.38	13.81	14.83
		+0.7% at t= 16 s	-6.961	28.18	-6.922	29.72	-5.143	28.57
		+1.3% at t= 40 s	-13.11	-	-13.11	-	-20.41	-
		-2% at t= 50s	21.82	66.64	20.87	63.70	26.12	65.84
		+1.2% at t= 70 s	-11.76	82.62	-12.09	83.88	-17.72	86.18

Table 8
State-of-the-Art comparison for the two area multi-source system (Dynamic Turbine thermal plant and Renewable sources) with step load perturbation applied

	Case/Controller	ΔF_1		ΔF_2		ΔP_{tie}	
		Over/Under Shoot	Settling Time (2%)	Over/Under Shoot	Settling Time (2%)	Over/Under Shoot	Settling Time (2%)
Case -I	I [23]	19.28×10^{-3}	41.34	17.81×10^{-3}	41.59	39.48×10^{-4}	41.92
	C-PID: (hITLBO-DE) [23]	5.775×10^{-3}	15.83	4.519×10^{-3}	15.27	9.365×10^{-4}	14.22
	$AP_1(\%)$	70.05	61.71	74.63	63.28	76.28	66.09
	PID: TLBO [9]	-22.06×10^{-3}	18.22	-16.02×10^{-3}	18.88	-8.19×10^{-4}	16.28
	IDD: TLBO [9]	-21.14×10^{-3}	17.95	-14.16×10^{-3}	18.72	-7.28×10^{-4}	13.01
	PIDD: TLBO [9]	-19.25×10^{-3}	16.14	-11.84×10^{-3}	16.79	-5.92×10^{-4}	12.77
	C-PID: hITLBO-DE [9]	-16.67×10^{-3}	7.91	-11.00×10^{-3}	8.76	-4.36×10^{-4}	8.68
	$AP_2(\%)$	13.40	50.99	7.09	47.83	26.35	32.03
	C-PID: (hITLBO-DE) With RFB in area-1, 2	-8.484×10^{-3}	12.97	-6.035×10^{-3}	16.29	-1.608×10^{-4}	12.26
	$AP_3(\%)$	55.93	19.64	49.03	2.98	72.84	3.99

to the system discussed in [23], considering the results of I controller [23] as reference.

The results obtained for the proposed C-PID control technique implemented to the multi-source system in [9] is compared to that of controllers such as PIDD, IDD, PID tuned by TLBO that were discussed in [9]. $AP_2(\%)$ represents the percentage improvement in system response achieved by the proposed C-PID: hITLBO-DE when applied to the system discussed in [9], considering the results of PIDD controller tuned by TLBO [23] as reference. The results for PIDD controller are considered as reference as it produces best result among PID: TLBO, IDD: TLBO, and PIDD: TLBO. The results obtained by the application of C-PID controller tuned by hITLBO-DE algorithm to the proposed system configuration in Fig. 1 is compared to that of [23] and [9]. $AP_3(\%)$ is evaluated by considering PIDD: TLBO as a reference as the Over/Under shoot and Settling time of PIDD: TLBO [9] is better as compared to that of [23].

To perform a fair comparison, in Table- 9, the proposed C-PID controller tuned by hITLBO-DE is applied to the

Table 9
State-of-the-Art comparison for the two area multi-source system (Dynamic Turbine thermal plant and Renewable sources) with dynamic load perturbation applied

Case/Controller			ΔF_1		ΔF_2		ΔP_{tie}	
		Various operating conditions	Over/under shoot ($\times 10^{-3}$)	Settling time (2%)	Over/under shoot ($\times 10^{-3}$)	Settling time (2%)	Over /under shoot ($\times 10^{-4}$)	Settling time (2%)
Case -V	I [23]	+0.5% at t= 16 s	-18.32	-	-23.35	-	-34.37	-
		+0.5% at t= 40 s	-18.32	-	-25.47	-	-36.28	-
		-1% at t= 50s	-19.24	-	-30.14	-	-38.59	-
		+0.7% at t= 70 s	-22.18	-	-30.28	-	-41.67	-
	C-PID: (hITLBO-DE) [23]	+0.5% at t= 16 s	-12.764	30.15	-18.25	30.19	-28.72	31.11
		+0.5% at t= 40 s	-12.764	-	-20.27	-	-29.38	-
		-1% at t= 50s	-14.251	66.42	-24.54	65.97	-32.39	64.85
		+0.7% at t= 70 s	-18.669	85.94	-25.08	86.39	-33.47	83.59
	C-PID: (hITLBO-DE)	+0.5% at t= 16 s	-4.231	27.28	-4.227	27.91	-16.02	28.20
		+0.5% at t= 40 s	-4.231	-	-4.227	-	-16.02	-
		-1% at t= 50s	8.621	62.69	8.618	62.73	32.75	62.58
		+0.7% at t= 70 s	5.934	82.67	-5.931	83.36	-22.47	82.60

system discussed in [23] and it is clearly observed that the proposed scheme is able to improve the system response significantly. Table- 9 compares the system response in terms of Over/Under shoot and 2% Settling time, for a dynamic load disturbance implemented with the C-PID controller tuned by hITLBO-DE algorithm to that obtained in [23] by application of I controller. So, it can be concluded that the proposed system configuration in Fig. 1 has higher degree of stability as compared to that in [23]. Considering AP_1, AP_2, and AP_3, the proposed scheme of C-PID controller and hITLBO-DE algorithm improves the system response under step load variations (Case-I, Case-II, Case-III, and Case-IV) and dynamic load variation (Case-V, Case-VI, and Case-VII). A improvement of 7.09 to 76.28% on Over/Under Shoot and 2.98 to 66.09% on Settling Time is achieved through application of C-PID controller and hITLBO-DE algorithm.

7. Conclusion

The stability analysis of a dynamic steam turbine system, with communication time delay, BSS and NCES, regulated by the formulated C-PID controller is presented in this paper. The ability of the system under perturbation, to regain a stable operating condition firmly depends on the performance of the controller and optimization technique. A C-PID controller tuned by a hITLBO-DE algorithm is formulated for enhancing the system stability when subjected to perturbation. Due to fast convergence characteristics of the hITLBO-DE algorithm, it is able to produce optimum controller parameters value within lesser computational time. Hence, from the performance and stability analysis it can be observed that the overshoot/undershoot and settling time of the system response is significantly improved as compared to the existing schemes. The major conclusions are listed below:

1. In the proposed power system model, NCES and BSS have been included to improve the system dynamics during peak load period.
2. Root locus, Bode plot, and eigenvalue analysis reflect the designed system to be stable. The damping ratio being within the range [0, 1] and a low oscillation frequency signifies good stability of the designed system.
3. The performance of the system is analyzed for cases of communication delay to determine the withstand capacity of the system. It is observed that the formulated C-PID controller is able to retain stable operation even for communication delay of 4 seconds.
4. It is observed that the C-PID controller is effective at suppressing any deviation in frequency and tie-line power caused by generation-demand imbalance and under a varying communication delay scenario. Amelioration of up to 76.28% on Over/Under Shoot and 66.09% on Settling Time is achieved through application of C-PID controller and hITLBO-DE algorithm.

8. Appendix

Steam turbine based dynamic model

Rating of machine = 500 MW; Equivalent speed droop characteristic R_{equ}=2.4 Hz/MW; Synchronizing coefficient $2\pi T_{12} = 0.545$ p.u.; Area capacity ratio a_{12} = -2; Bias factor $B_i = 0.433$; Governor time constant = 0.008 sec; Time constant delay of crossover $T_{co} = 0.400$ sec; Time constant delay of re-heater $T_{RH} = 5.000$ sec; Time constant delay of steam chest $T_{sc} = 0.2999$ sec; Power fraction of low pressure turbine $F_{LP} = 0.3760$; Power fraction of intermediate pressure turbine $F_{IP} = 0.3511$; Power fraction of high pressure turbine $F_{HP} = 0.2727$; Power system gain K_{PS} = 120; Power system time constant $T_{PS} = 20.00$ sec.

Hydro power plant

Governor time constant $T_{GH} = 48.7$ sec; Turbine time constant $T_{RSi} = 0{:}513$ sec; $T_{RHi} = 10$ sec; $T_{Wi} = 1$ sec.

Gas power plant

Gas turbine time constant c_g,b_g, X_e, Y_e, T_{CR}, T_F, T_{CD} = 0.049 sec, 0.6 sec, 1.1 sec, 0.01 sec, 0.239 sec, 0.2 sec respectively.

Solar PV power plant

Gain $k = 4.64$; Time constant of PV $T_{pv} = 0.054$ sec.

Wind turbine generator

Hydraulic pitch actuator gain $K_{p2} = 1.25$: Hydraulic pitch actuator time constant T_{p1}, T_{p2} = 0.60 sec, 0.041 sec respectively: Data-fit pitch response $K_{p3} = 1.40$; Blade characteristics $K_{pc} = 0.80$.

Battery storage system

Gain of RFB $K_{RFB} = 0.6787$, Time constant of RFB $T_{RFB} = 0$ sec.

References

[1] O. Elgerd, Electric energy systems theory an introduction, McGraw-Hill Book Company, New York, NY, 2000.

[2] H. Bevrani, Robust power system frequency control, volume 85, Springer, 2009.

[3] W. Tan, Decentralized load frequency controller analysis and tuning for multi-area power systems, Energy Conversion and Management 52 (2011) 2015–2023.

[4] L. C. Saikia, J. Nanda, S. Mishra, Performance comparison of several classical controllers in agc for multi-area interconnected thermal system, International Journal of Electrical Power & Energy Systems 33 (2011) 394–401.

[5] E. Ali, S. Abd-Elazim, Bfoa based design of pid controller for two area load frequency control with nonlinearities, International Journal of Electrical Power & Energy Systems 51 (2013) 224–231.

[6] R. K. Sahu, S. Panda, S. Padhan, A hybrid firefly algorithm and pattern search technique for automatic generation control of multi area power systems, International Journal of Electrical Power & Energy Systems 64 (2015) 9–23.

[7] K. S. Parmar, S. Majhi, D. Kothari, Load frequency control of a realistic power system with multi-source power generation, International Journal of Electrical Power & Energy Systems 42 (2012) 426–433.

[8] B. K. Sahu, S. Pati, P. K. Mohanty, S. Panda, Teaching–learning based optimization algorithm based fuzzy-pid controller for automatic generation control of multi-area power system, Applied Soft Computing 27 (2015) 240–249.

[9] R. K. Sahu, T. S. Gorripotu, S. Panda, Automatic generation control of multi-area power systems with diverse energy sources using teaching learning based optimization algorithm, Engineering Science and Technology, an International Journal 19 (2016) 113–134.

[10] P. Dash, L. C. Saikia, N. Sinha, Automatic generation control of multi area thermal system using bat algorithm optimized PD–PID cascade controller, International Journal of Electrical Power & Energy Systems 68 (2015) 364–372.

[11] P. Dash, L. C. Saikia, N. Sinha, Flower pollination algorithm optimized PI-PD cascade controller in automatic generation control of a multi-area power system, International Journal of Electrical Power & Energy Systems 82 (2016) 19–28.

[12] M. Elsisi, M. Soliman, M. Aboelela, W. Mansour, Improving the grid frequency by optimal design of model predictive control with energy storage devices, Optimal Control Applications and Methods 39 (2018) 263–280.

[13] K. S. Simhadri, B. Mohanty, S. K. Panda, Comparative performance analysis of 2dof state feedback controller for automatic generation control using whale optimization algorithm, Optimal Control Applications and Methods 40 (2019) 24–42.

[14] Y. Arya, N. Kumar, Agc of a two-area multi-source power system interconnected via ac/dc parallel links under restructured power environment, Optimal Control Applications and Methods 37 (2016) 590–607.

[15] Y. Arya, N. Kumar, Optimal control strategy–based agc of electrical power systems: A comparative performance analysis, Optimal Control Applications and Methods 38 (2017) 982–992.

[16] R. Shankar, A. Kumar, U. Raj, K. Chatterjee, Fruit fly algorithm-based automatic generation control of multiarea interconnected power system with facts and ac/dc links in deregulated power environment, International Transactions on Electrical Energy Systems (2018) e2690.

[17] B. Wang, J. Xu, R. Wai, B. Cao, Adaptive sliding-mode with hysteresis control strategy for simple multimode hybrid energy storage system in electric vehicles, IEEE Transactions on Industrial Electronics 64 (2017) 1404–1414.

[18] B. Wang, D. Zhao, W. Li, Z. Wang, Y. Huang, Y. You, S. Becker, Current technologies and challenges of applying fuel cell hybrid propulsion systems in unmanned aerial vehicles, Progress in Aerospace Sciences 116 (2020) 100620.

[19] T. Panigrahi, P. Dash, P. Hota, A self-tuning optimised unscented kalman filter for voltage flicker and harmonic estimation, Int. J. of Power and Energy Conversion 2 (2010) 250–278.
[20] X. Wu, K. Zhang, M. Cheng, X. Xin, A switched dynamical system approach towards the economic dispatch of renewable hybrid power systems, International Journal of Electrical Power & Energy Systems 103 (2018) 440–457.
[21] A. Barisal, T. Panigrahi, S. Mishra, A hybrid pso-levy flight algorithm based fuzzy pid controller for automatic generation control of multi area power systems: Fuzzy based hybrid pso for automatic generation control, Int. J. of Power and Energy Conversion 6 (2017) 42–63.
[22] N. Pathak, A. Verma, T. S. Bhatti, Automatic generation control of thermal power system under varying steam turbine dynamic model parameters based on generation schedules of the plants, The Journal of Engineering 2016 (2016) 302–314.
[23] N. Pathak, T. S. Bhatti, A. Verma, Accurate modelling of discrete agc controllers for interconnected power systems, IET Generation, Transmission & Distribution 11 (2017) 2102–2114.
[24] G. S. Sisodia, P. Singh, The status of renewable energy research on india, Energy Procedia 95 (2016) 416 – 423. International Scientific Conference on Environmental and Climate Technologies, CONECT 2015.
[25] S. Lolla, S. B. Roy, S. Chowdhury, Wind and solar energy resources in india, Energy Procedia 76 (2015) 187 – 192. European Geosciences Union General Assembly 2015 - Division Energy, Resources and Environment, EGU 2015.
[26] K. Sopian, A. Fudholi, M. H. Ruslan, M. Y. Sulaiman, M. A. Alghoul, M. Yahya, N. Amin, L. C. Haw, A. Zaharim, Optimization of a stand-alone wind/pv hybrid system to provide electricity for a household in malaysia, in: 4th IASME/WSEAS International Conference on Energy & Environment, Algarve, Portugal, June, xxyyzz, 2009, pp. 11–13.
[27] R. Kadri, J.-P. Gaubert, G. Champenois, An improved maximum power point tracking for photovoltaic grid-connected inverter based on voltage-oriented control, IEEE Transactions on Industrial Electronics 58 (2011) 66–75.
[28] M. Rezkallah, S. K. Sharma, A. Chandra, B. Singh, D. R. Rousse, Lyapunov function and sliding mode control approach for the solar-pv grid interface system, IEEE Transactions on Industrial Electronics 64 (2017) 785–795.
[29] D. Das, S. Aditya, D. Kothari, Dynamics of diesel and wind turbine generators on an isolated power system, International Journal of Electrical Power & Energy Systems 21 (1999) 183 – 189.
[30] P. Dahiya, P. Mukhija, A. R. Saxena, Y. Arya, Comparative performance investigation of optimal controller for agc of electric power generating systems, Automatika: časopis za automatiku, mjerenje, elektroniku, računarstvo i komunikacije 57 (2016) 902–921.
[31] P. Hota, B. Mohanty, Automatic generation control of multi source power generation under deregulated environment, International Journal of Electrical Power & Energy Systems 75 (2016) 205–214.
[32] S. Dhundhara, Y. P. Verma, Evaluation of ces and dfig unit in agc of realistic multisource deregulated power system, International Transactions on Electrical Energy Systems 27 (2017) e2304.
[33] S. M. Shinners, Modern Control System Theory and Design, John Wiley & Sons, Inc., New York, NY, USA, 1998.
[34] B. K. Huang, Computer simulation analysis of biological and agricultural systems, CRC Press, Boca Raton, Florida, 1994.
[35] J. N. Bharothu, M. Sridhar, R. S. Rao, Modified adaptive differential evolution based optimal operation and security of ac-dc microgrid systems, International Journal of Electrical Power & Energy Systems 103 (2018) 185–202.
[36] T. Panigrahi, A. Behera, Operation of automatic voltage regulator (avr) under single fault and cascaded fault condition, Int. J. of Research and Scientific Innovation (IJRSI) 3 (2016) 32–37.
[37] D. Chen, F. Zou, Z. Li, J. Wang, S. Li, An improved teaching–learning-based optimization algorithm for solving global optimization problem, Information Sciences 297 (2015) 171–190.
[38] R. Khadanga, A. Kumar, Hybrid adaptive gbest-guided gravitational search and pattern search algorithm for automatic generation control of multi-area power system, IET Generation, Transmission and Distribution 11 (2016) 3257 âĂŞ 3267.
[39] B. Mohanty, B. Acharyulu, P. Hota, Moth-flame optimization algorithm optimized dual-mode controller for multiarea hybrid sources agc system, Optimal Control Applications and Methods 39 (2018) 720–734.